



Contents lists available at ScienceDirect

Journal of the Mechanics and Physics of Solids

journal homepage: www.elsevier.com/locate/jmps

Elastic Cherenkov effects in transversely isotropic soft materials-I: Theoretical analysis, simulations and inverse method

Guo-Yang Li^a, Yang Zheng^a, Yanlin Liu^a, Michel Destrade^b, Yanping Cao^{a,*}^a Institute of Biomechanics and Medical Engineering, AML, Department of Engineering Mechanics, Tsinghua University, Beijing 100084, PR China^b School of Mathematics, Statistics and Applied Mathematics, National University of Ireland Galway, Galway, Ireland

ARTICLE INFO

Article history:

Received 2 November 2015

Received in revised form

31 March 2016

Accepted 17 May 2016

Available online 25 June 2016

Keywords:

Elastic Cherenkov effect (ECE)

Anisotropic soft materials

Dynamic elastography

Supersonic shear imaging (SSI) technique

Inverse method

ABSTRACT

A body force concentrated at a point and moving at a high speed can induce shear-wave Mach cones in dusty-plasma crystals or soft materials, as observed experimentally and named the elastic Cherenkov effect (ECE). The ECE in soft materials forms the basis of the supersonic shear imaging (SSI) technique, an ultrasound-based dynamic elastography method applied in clinics in recent years. Previous studies on the ECE in soft materials have focused on isotropic material models. In this paper, we investigate the existence and key features of the ECE in anisotropic soft media, by using both theoretical analysis and finite element (FE) simulations, and we apply the results to the non-invasive and non-destructive characterization of biological soft tissues. We also theoretically study the characteristics of the shear waves induced in a deformed hyperelastic anisotropic soft material by a source moving with high speed, considering that contact between the ultrasound probe and the soft tissue may lead to finite deformation. On the basis of our theoretical analysis and numerical simulations, we propose an inverse approach to infer both the anisotropic and hyperelastic parameters of incompressible transversely isotropic (TI) soft materials. Finally, we investigate the properties of the solutions to the inverse problem by deriving the condition numbers in analytical form and performing numerical experiments. In Part II of the paper, both *ex vivo* and *in vivo* experiments are conducted to demonstrate the applicability of the inverse method in practical use.

© 2016 Elsevier Ltd. All rights reserved.

1. Introduction

The systematic theoretical treatment of waves generated in an infinite elastic solid by a variable body force dates back to the classic work of Eason et al. (1956). In the introduction of that paper, the authors made the following remark regarding their theoretical solutions, which seemed reasonable at that time: “*In many cases, too, it is difficult to see how the solutions as they stand can be applied to a practical engineering problem. A body force concentrated at a point and moving with uniform velocity through an infinite solid is not easy to envisage physically.*” Approximately 50 years after the publication of that seminal paper, experiments on wave motion in a dusty-plasma crystal clearly demonstrated shear-wave Mach cones

* Corresponding author.

E-mail address: caoyanping@tsinghua.edu.cn (Y. Cao).

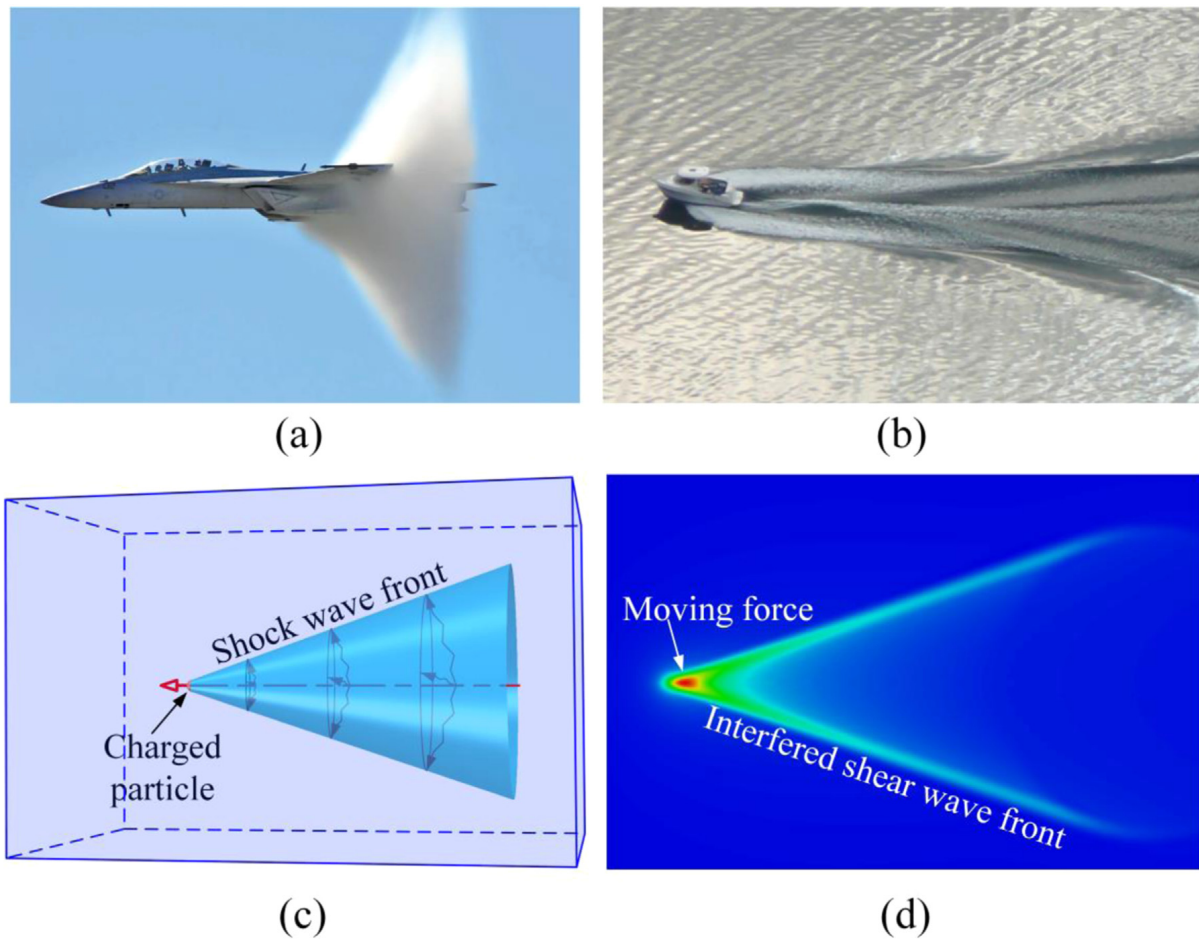


Fig. 1. Four similar wave phenomena in which the velocity of the excitation source is greater than that of the resulting waves in the medium. (a) “Sonic boom” phenomenon caused by an F/A-18F plane during a transonic flight, (b) the wake pattern generated by a high-speed yacht, (c) a schematic of Cherenkov radiation, (d) the ECE induced by a moving shear source in soft media.

generated by a laser radiation force moving with a high speed (Melzer et al., 2000; Nosenko et al., 2002). Subsequently, a French group (Bercoff et al., 2004a, 2004b) proposed a technique to generate a concentrated body force moving with supersonic speed through soft media to generate shear-wave Mach cones. Their key idea was to use ultrasonic focused beams to remotely generate a mechanical vibration source inside the soft medium. The vibration source can move at supersonic speed along a given direction, and the resulting shear waves interfere constructively along a Mach cone according to the theory developed by Eason et al. (1956), thus creating two intense plane shear waves (Fig. 1d). This phenomenon is analogous to the “sonic boom” created by a supersonic aircraft (Fig. 1a), the wake patterns generated by a high-speed yacht (Fig. 1b) (Rabaud and Moisy, 2013) and the Cherenkov effects induced by a high-energy charged particle passing through a transparent medium at a speed greater than the speed of light in that medium (Fig. 1c). Hence, Bercoff et al. (2004a, 2004b) have named the phenomenon observed in their experiments the elastic Cherenkov effect (ECE, Fig. 1d), and it forms the theoretical basis of the supersonic shear imaging (SSI) technique.

The SSI technique (Bercoff et al., 2004a) is a shear wave elastography (SWE) method that has received considerable attention since the 1990s (Sarvazyan et al., 1998; Fatemi and Greenleaf, 1998; Nightingale et al., 2002; Chen et al., 2009a; Song et al., 2012, 2015). SWE methods using shear waves traveling in human soft tissues to deduce *in vivo* elastic properties have found widespread clinical applications, including monitoring the development of liver fibrosis, detecting malignant tumors, assessing myocardial elasticity, and determining the stage of chronic kidney disease (CKD).

Liver fibrosis is a common pathway for a multitude of liver injuries. Precisely estimating the degree of liver fibrosis is of great importance for the evaluation of prognosis, surveillance, and treatment decisions in patients with chronic liver disease (Chen et al., 2009b; Bavu et al., 2011; Ferraioli et al., 2012; Bota et al., 2013; Cassinotto et al., 2013; Paparo et al., 2014). Currently, liver biopsy is the reference standard for the assessment of liver fibrosis. However, it is an invasive method associated with patient discomfort, and its accuracy is limited by intra- and inter-observer variability and sampling error. Therefore, the development of a non-invasive method, such as elastography, to inspect the occurrence and development of liver fibrosis is urgently needed. Tumors are frequently detected through physical palpation as hard masses located within surrounding softer tissues. Elastography methods may serve as a “virtual finger” allowing quantitative detection of the

stiffness of the solid tumor and has the potential to differentiate malignant tumors from benign ones (Bercoff et al., 2004a; Tanter et al., 2008; Athanasiou et al., 2010; Chamming's et al., 2013). Cardiac pathologies, including postinfarction remodeling and hypertrophic cardiomyopathy, are usually accompanied by fibrosis and myocardial fiber disorganization. Therefore, evaluating the myocardial elasticity and myocardial fiber orientation may help diagnose hypertrophic or ischemic cardiomyopathy (Lee et al., 2012). CKD is difficult to diagnose by using conventional medical imaging methods. It has been recognized that intra-renal fibrosis is a final common pathway for all CKD and can alter renal stiffness. SWE methods enable assessment of the renal stiffness and can therefore provide valuable diagnostic information in CKD (Samir et al., 2015).

The SSI technique is distinct from other SWE methods in that it relies on the ECE induced in isotropic soft media. Moreover, it uses an ultrafast imaging technique to visualize and measure the speed of the resulting shear wave in less than 20 ms (Bercoff et al., 2004a, 2004b). In principle, this measurement enables mapping of the elasticity of the tissue, once the wave speed is related to the tissue stiffness. This technique has great potential in the diagnosis of some diseases; however, some fundamental issues remain regarding the clinical use of the SSI technique, and these issues warrant careful investigation. This paper is concerned with the following issues.

First, it is well known that most soft biological tissues are anisotropic materials; this category includes the cardiovascular system, skin, kidneys and muscles. The use of the SSI technique on these soft organs/tissues requires revealing and understanding the salient features of the ECE in *anisotropic* soft media and no systematic studies have yet been performed to address this important issue to the authors' knowledge. *Second*, by modeling soft tissues as incompressible transversely isotropic (TI) materials, a number of authors (Genin et al., 2010, 2012) have recently attempted to determine the anisotropic elastic properties of the kidney and skeletal muscles by using the SSI technique but without exploring the ECE. It should be pointed out that three constitutive parameters are required to describe an incompressible TI linear elastic solid; generally, these are the transverse and longitudinal shear moduli and the elastic modulus. The studies above (Genin et al., 2010, 2012) have assessed the shear moduli μ_T and μ_L , but have not evaluated the *elastic modulus* E_L by using the SSI technique. *Third*, contact between the probe and the soft tissue may lead to finite deformation of the medium. In this case, the propagation of the shear wave generated by a moving source in a *deformed* anisotropic soft tissue should be investigated. The resulting study of this acousto-elastic effect will enable quantitative evaluation of the effects of finite deformation on the determination of the anisotropic properties of soft tissues by using the SSI technique. Furthermore, it may also be used to develop an inverse approach to determine the *in vivo* hyperelastic properties of an anisotropic soft tissue.

Bearing the above issues in mind, we investigated the ECE in an incompressible TI material, which has widely been adopted to model soft tissues, and we propose an inverse approach to infer both the linear anisotropic elastic parameters and the hyperelastic parameters of the material. Part I of the paper is organized as follows. Section 2 presents the elastodynamic model describing the elastic waves generated in an anisotropic elastic medium by a pulse load and a uniformly moving point force. We give the dispersion relation of the TI elastic medium, which can be used to determine the correlation between the phase velocities and the group velocities of the shear waves induced by the moving point force. We then conduct a theoretical analysis in Section 3 to derive the displacement field caused by a moving point force in both isotropic elastic solids and a special anisotropic elastic medium. The results provide considerable insights into the ECE in these cases, for instance giving the shape of the Mach cone and the critical moving speed of the vibration source (*i.e.*, the focused acoustic radiation force) beyond which the quasi-plane waves can be generated. To reveal the salient features of the ECE in more general TI soft media, we develop a finite element (FE) model in Section 4 to solve the elastodynamic problem with a vibration source moving at different speeds in a TI solid. In Section 5, we perform a theoretical analysis based on the incremental elastodynamic theory (Ogden, 2007) and derive an analytical solution to elucidate the influence of finite deformation on the propagation of shear waves in an incompressible TI solid. Based on the analysis conducted in Sections 3–5, we propose an inverse method in Section 6 to determine the anisotropic and hyperelastic parameters of TI soft materials by using the SSI technique. We conduct both a theoretical analysis and numerical experiments to investigate the properties of the solutions to the present inverse problem. Finally we provide some concluding remarks in Section 7. In Part II of the paper (Li et al., 2016), *ex vivo* and *in vivo* experiments are performed to validate our inverse method and demonstrate its usefulness in practice.

2. Wave motion in a TI soft medium

The elastodynamic equations and corresponding dispersion relations involved in this study are briefly given in this section, and one can refer to Achenbach (1973) and Auld (1990) for details.

The equilibrium equations under the assumption of infinitesimal deformation are given by

$$c_{ijkl}u_{k,jl} + f_i = \rho u_{i,tt}, \quad (2.1)$$

where u_i ($i = 1, 2, 3$) are the components of the displacement, c_{ijkl} are the components of the fourth-order elastic tensor, and f_i are the components of the body force. ρ is the mass density, and t the time. The subscript ' t ' represents the material time derivative. Here, the stress-strain relation is given by $\sigma_{ij} = c_{ijkl}\epsilon_{kl}$, and the strain components ϵ_{kl} are related to the displacement by $\epsilon_{kl} = \frac{1}{2}(u_{k,l} + u_{l,k})$. The fundamental solution corresponding to the pulse load is usually referred to as the elastodynamic *Green function*, which can be used to derive the solutions for variable loads (Wu, 2002). Suppose that the

body force is a pulse force imposed at the origin of the coordinates and along the direction of \mathbf{e}_m , where \mathbf{e}_m is the base vector of x_m ($m = 1, 2, 3$), i.e., $f_i = \delta(\mathbf{x})\delta(t)\delta_{im}$, where $\delta(\mathbf{x})$ is the delta function and δ_{im} is the Kronecker delta. Then, Eq. (2.1) can be written as

$$c_{ijkl}u_{k,jl} + \delta(\mathbf{x})\delta(t)\delta_{im} = \rho u_{i,tt}. \quad (2.2)$$

The solution to Eq. (2.2) is denoted by $G_{im}(\mathbf{x}, t)$, and thus, Eq. (2.1) can be written as

$$c_{ijkl}G_{km,jl} + \delta(\mathbf{x})\delta(t)\delta_{im} = \rho G_{im,tt}. \quad (2.3)$$

The subscript ‘ m ’ of the Green function G_{im} refers to the loading direction of the point force. G_{im} can be solved in analytical form for an infinite isotropic solid and some special anisotropic solids (Aki and Richards, 1980; Wang and Achenbach, 1994; Vavryčuk, 2001).

To derive the wave dispersion relationships, we consider plane waves in the form

$$u_i(\mathbf{x}, t) = U_i \exp[i(\mathbf{k} \cdot \mathbf{x} - \omega t)], \quad (2.4)$$

where $\mathbf{k} = k\hat{\mathbf{k}}$ is the wave vector, and $k = |\mathbf{k}|$ the wave number. ω represents the circular frequency, U_i is the amplitude of the wave along \mathbf{e}_i , and the direction of the vector $\mathbf{U} = U_i\mathbf{e}_i$ is referred to as the polarization direction of the wave. Inserting Eq. (2.4) into the equilibrium equation, the following relation can be obtained

$$\left(k^2 c_{ijkl} \hat{k}_j \hat{k}_l - \rho \omega^2 \delta_{ik}\right) U_k = 0. \quad (2.5)$$

The existence of a non-zero U_k requires

$$\det\left(k^2 c_{ijkl} \hat{k}_j \hat{k}_l - \rho \omega^2 \delta_{ik}\right) = 0, \quad (2.6)$$

where ‘det’ represents the determinant. It should be noted that Eq. (2.6) is a homogeneous equation, so that $\omega(\mathbf{k}) = \omega(k\hat{\mathbf{k}}) = k\omega(\hat{\mathbf{k}})$ (Landau and Lifshitz, 1986). The function $\omega(\hat{\mathbf{k}})$ gives the dispersion relation. Then, the phase velocity v reads

$$v = \frac{\omega(\mathbf{k})}{k} = \omega(\hat{\mathbf{k}}), \quad (2.7)$$

which is independent of ω . The group velocity, which represents the velocities of the wave packets, is a vector and given by

$$\mathbf{v}_g = \frac{\partial \omega}{\partial \mathbf{k}}. \quad (2.8)$$

In this study, we focus on an incompressible TI linear elastic material model. It has three independent material constants (Spencer, 1984; Chadwick, 1993; Destrade et al., 2002; Rouze et al., 2013; also see the Supporting Information (SI) 1), taken here as μ_L and E_L , the initial shear modulus and extension modulus along the fiber direction, respectively, and μ_T , the shear modulus perpendicular to that direction. In this section and henceforth, we choose a Cartesian coordinate system such that its x_3 -axis is aligned with the fibers, and x_1 and x_2 are arbitrarily chosen in the perpendicular plane (Fig. 2a). In this coordinate system, the relationships between the elastic stiffnesses c_{ijkl} and μ_L , μ_T and E_L are straightforward to derive (see SI1). The dispersion relations for incompressible TI materials can be obtained by inserting those relationships into Eq. (2.6).

For incompressible TI materials, Chadwick (1993) has established that two transverse waves may propagate in the medium (Carcione, 2007; Papazoglou et al., 2006; see also SI1), with speeds given by

$$\begin{cases} \rho v_{SH}^2 = \mu_T \left(\hat{k}_1^2 + \hat{k}_2^2 \right) + \mu_L \hat{k}_3^2 \\ \rho v_{qSV}^2 = \mu_L + (E_L + \mu_T - 4\mu_L) \left(1 - \hat{k}_3^2 \right) \hat{k}_3^2 \end{cases} \quad (2.9)$$

where we follow the geophysics convention for the subscripts ‘SH’ and ‘SV’ (Thomsen, 1986). The first (shear horizontal) wave is a pure transverse mode, polarized along $\mathbf{e}_3 \times \hat{\mathbf{k}}$, whereas the second (quasi-shear vertical) is polarized approximately along $\mathbf{e}_3 \times \hat{\mathbf{k}} \times \hat{\mathbf{k}}$.

The two shear modes may be involved simultaneously in the use of the SSI technique. In previous studies (Gennisson et al., 2010; Lee et al., 2012; Eby et al., 2015), the axis of the ultrasound probe is perpendicular to the fibers, so that the resulting shear waves are the SH modes according to the definition above. Rotating the probe about its axis (see Fig. 2b) changes the shear wave speeds continuously, thus giving access to the linear anisotropic properties of muscles (Gennisson et al., 2010; Lee et al., 2012). However, Eq. (2.9) shows that the phase velocities of the SH mode depend only on the two elastic parameters μ_T and μ_L and that the protocol does not yield the parameter E_L . Bearing this issue in mind, and inspired

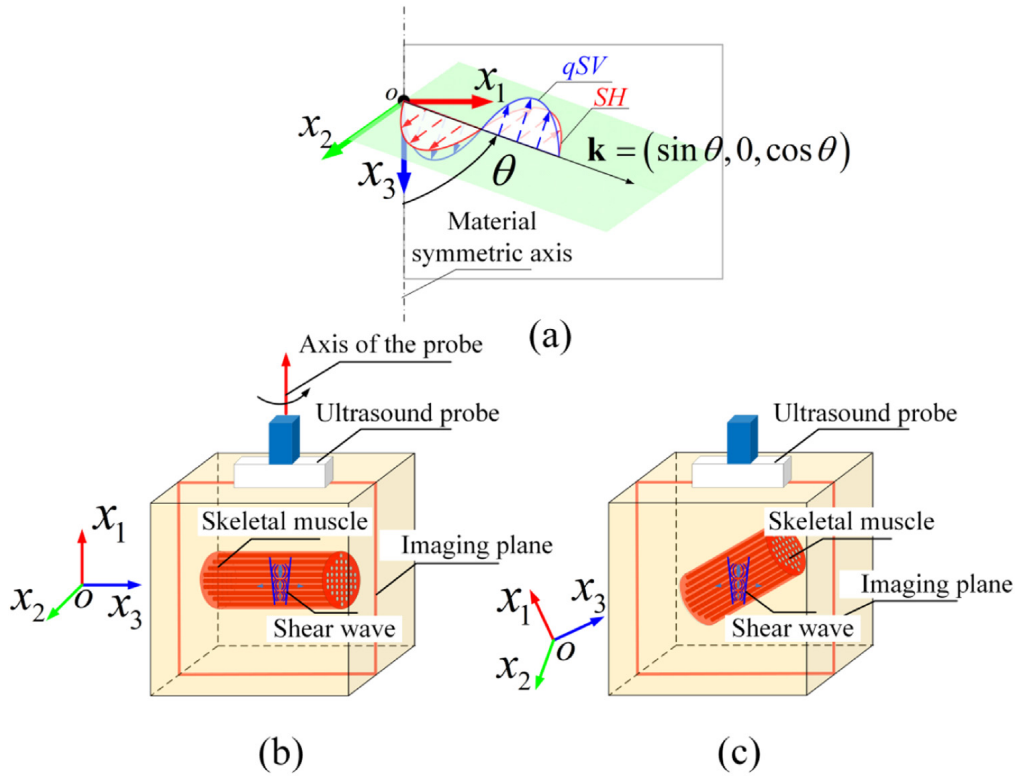


Fig. 2. Schematic of shear waves of the SH and qSV modes and measurements of skeletal muscle by using the SSI technique. (a) Schematic of the SH mode and the qSV mode. θ denotes the angle between the wave vector \mathbf{k} and x_3 -axis, so that $\mathbf{k} = (\sin \theta, 0, \cos \theta)$. (b) Using the shear waves of the SH mode to measure the elastic parameters of skeletal muscle. By rotating the ultrasound probe, the velocities of the SH mode shear wave can be measured in different directions. (c) Experimental setup proposed in this study to measure E_L . The polarization directions of the shear waves are no longer perpendicular to the material symmetric direction, and the shear waves are qSV modes.

by the work of Rouze et al. (2013), we propose a method based on the SSI technique to determine E_L by using the qSV mode. The key idea is shown in Fig. 2c. Indeed, when the axis of the ultrasound probe is not perpendicular to the fibers, neither are the polarization directions of the resulting shear waves. In this case, the shear wave of the qSV mode can be evaluated by using the SSI technique, which can be related to the parameter E_L , as shown in detail below.

To illustrate the dependence of the shear wave speeds of the qSV mode on the elastic parameter E_L , we introduce the following parameter C

$$C = \frac{E_L + \mu_T - 4\mu_L}{2}, \tag{2.10}$$

so that from Eq. (2.9), we have

$$\rho v_{qSV}^2 = \mu_L + 2C \left(1 - \hat{k}_3^2 \right) \hat{k}_3^2. \tag{2.11}$$

In Fig. 3, the spatial distributions of the phase velocities of the qSV mode shear waves are plotted for different propagation directions. It can be seen that the distribution of the wave speeds depends strongly on the parameter C . In general, Eq. (2.11) indicates that it is possible to infer E_L from v_{qSV} once μ_T and μ_L are known from the measurements of v_{SH} , provided that the ECE exists in an incompressible TI solid.

3. Theoretical analysis of the ECE

The ECE forms the theoretical basis of the SSI technique. To date, experimental evidence of the ECE has been reported in isotropic elastic solids (Bercoff et al., 2004a, 2004b), but its existence and key features in anisotropic elastic solids have not been fully investigated. In this section, we first briefly revisit the ECE in isotropic elastic solids. Although the results can also be obtained from the original theory by Eason et al. (1956), here, we base our derivations on the more recent treatments by Dowling and Williams (1983) and Bercoff et al. (2004b). Furthermore, we derive the theoretical and analytical solutions for the ECE in a special type of anisotropic elastic solid, namely, incompressible TI solids with $C = 0$. In Section 4, we develop a FE model to solve the elastodynamic problem and investigate the ECE in more general TI soft media with $C \neq 0$.

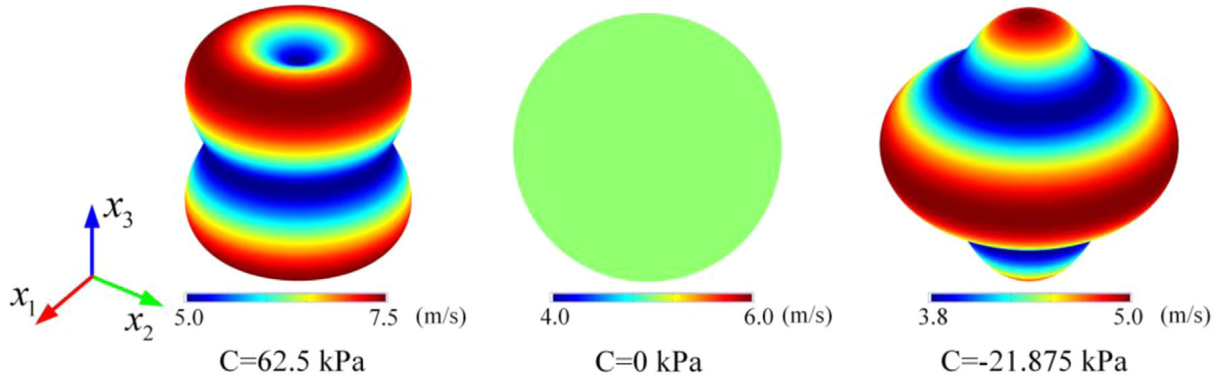


Fig. 3. Spatial distribution of the phase velocities for the shear wave of the qSV mode. For illustration, we take $\mu_T = 9$ kPa and $\mu_L = 25$ kPa for all three cases, and C (kPa) = 62.5, 0, - 21.875, respectively.

3.1. The ECE in an isotropic elastic soft medium

The displacement field induced by a variable body force f_i depends on the time t and position \mathbf{x} via the integral

$$u_i(\mathbf{x}, t) = \int \int f_m(\xi, \tau) G_{im}(\mathbf{x}-\xi, t-\tau) d\tau d\xi. \tag{3.1}$$

where G_{im} is the Green function (see Achenbach (1973) or Auld (1990) for details).

The uniformly moving point force is imposed along the same direction as its moving direction and thus can be written in the form

$$f_i(\mathbf{x}, t) = a_i \delta(\mathbf{x} - v_e \mathbf{t}), \tag{3.2}$$

where \mathbf{a} is the unit vector along the movement direction, and v_e is the movement speed. For an isotropic elastic solid with Lamé constants marked as λ and μ , the Green function is given by (Aki and Richards, 2002)

$$G_{im}^{Iso}(\mathbf{x}, t) = \frac{1}{4\pi\rho} (3\gamma_i\gamma_m - \delta_{im}) \frac{1}{r^3} \int_{r/v_p}^{r/v_s} \tau \delta(t-\tau) d\tau + \frac{1}{4\pi\rho v_p^2} \gamma_i\gamma_m \frac{1}{r} \delta\left(t - \frac{r}{v_p}\right) + \frac{1}{4\pi\rho v_s^2} (\delta_{im} - \gamma_i\gamma_m) \frac{1}{r} \delta\left(t - \frac{r}{v_s}\right). \tag{3.3}$$

where $r = |\mathbf{x}|$, $\gamma_i = \frac{x_i}{r} = \frac{\partial r}{\partial x_i}$, and $v_s = \sqrt{\mu/\rho}$, $v_p = \sqrt{(\lambda + 2\mu)/\rho}$ are the velocities of the S wave (shear wave, secondary wave) and P wave (pressure wave, primary wave) in isotropic elastic media, respectively. The superscript ‘Iso’ denotes isotropic materials. Neglecting the coupling components (the first term in Eq. (3.3)), because they decay quickly away from the sources (Aki and Richards, 2002), and the P wave term (the second term in Eq. (3.3)), because $v_p \gg v_s$ in an incompressible soft solid, Eq. (3.3) can be approximately written as

$$G_{im}^{Iso} \approx \frac{1}{4\pi\rho v_s^2} (\delta_{im} - \gamma_i\gamma_m) \frac{1}{r} \delta\left(t - \frac{r}{v_s}\right). \tag{3.4}$$

Without losing generality, let $\mathbf{a} = (0, 0, 1)$, which indicates that the force is moving along x_3 . Inserting Eqs. (3.4) and (3.2) into Eq. (3.1) (see SI2 for the detailed derivations), we have

$$u_i(\mathbf{x}, t) = \frac{1}{\sqrt{1 - M_{Iso}^2 \sin^2 \theta(t)}} F^{Iso}(\mathbf{x}, t, \tau_1^{Iso}, \tau_2^{Iso}), \tag{3.5}$$

where $M_{Iso} = v_e/v_s$ is defined as the Mach number,

$$\tau_{1,2}^{Iso} = t + \frac{R(t)}{v_s(M_{Iso}^2 - 1)} \left(M_{Iso} \cos \theta(t) \pm \sqrt{1 - M_{Iso}^2 \sin^2 \theta(t)} \right), \tag{3.6}$$

$$F^{Iso}(\mathbf{x}, t, \tau_1^{Iso}, \tau_2^{Iso}) = \sum_{k=1}^2 \frac{1}{4\pi\mu R(t)} \left(\delta_{i3} - \frac{\partial R(\tau_k^{Iso})}{\partial x_i} \frac{\partial R(\tau_k^{Iso})}{\partial x_3} \right). \tag{3.7}$$

and

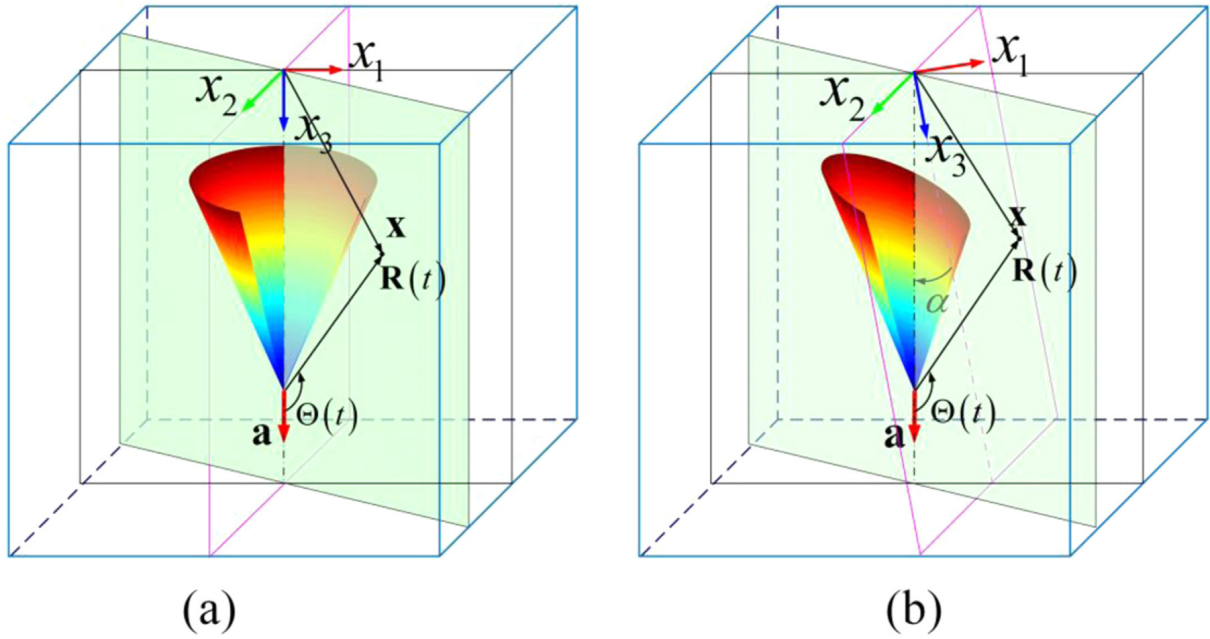


Fig. 4. A schematic of the ECE in a soft medium. (a) The ECE in an isotropic elastic solid. The force is moving along the x_3 -axis. The resulting displacements are confined in a Mach cone according to Eq. (3.5). (b) The ECE in an incompressible TI solid. The force is moving along $\mathbf{a} = (-\sin \alpha, 0, \cos \alpha)$ with velocity v_e . Here, only the Mach cone for the SH mode is plotted, and it is no longer a perfect cone for an anisotropic solid in the physical coordinate system.

$$\begin{cases} \mathbf{R}(t) = \mathbf{x} - v_e t \mathbf{a} \\ \theta(t) = \arccos\left(\frac{\mathbf{R} \cdot \mathbf{a}}{R}\right), \end{cases} \quad (3.8)$$

where $R(t) = |\mathbf{R}(t)|$ is the distance between a spatial point \mathbf{x} and the point where the moving force is applied at time t , and $\theta(t)$ is the angle between the vector \mathbf{a} and $\mathbf{R}(t)$ (Fig. 4a).

Eq. (3.6) shows that the following inequality must hold

$$1 - M_{iso}^2 \sin^2 \theta(t) \geq 0. \quad (3.9)$$

In the case of $M_{iso} > 1$, where the speed of the moving point force is greater than the velocity of the resulting shear waves, we thus have

$$|\sin \theta| \leq \frac{1}{M_{iso}}, \quad (3.10)$$

which indicates that the displacements are confined in a *Mach cone*. Furthermore, Eq. (3.5) shows that the displacements are singular on the cone surface. This is the ECE phenomenon, which has been demonstrated experimentally by [Bercoff et al. \(2004b\)](#).

3.2. The ECE in an incompressible TI soft medium with $C = 0$

A number of authors have investigated the response of an anisotropic elastic solid subjected to moving line forces ([Stroh, 1962](#); [Asaro et al., 1973](#); [Ting, 1996](#); [Wu, 2002](#); [Iovane et al., 2004, 2005](#)). In this paper, we perform an analytical study on the wave motion in an incompressible TI solid by considering a moving point force to reveal the key features of the ECE, which has not been done in previous studies.

Obtaining the dynamic *Green function* in Eq. (3.1) in analytical form for a general anisotropic elastic solid remains challenging; however, it is possible to obtain $G_{im}(\mathbf{x}, t)$ in analytical form for some special types of anisotropic elastic solids. For instance, for incompressible TI solids with $C = 0$, the *Green function* has been obtained through the high-order ray theory ([Vavryčuk, 2001](#)). Under the condition of incompressibility and neglecting the coupling components, the solution is

$$G_{im}^{TI}(\mathbf{x}, t) \approx \frac{1}{4\pi\rho^{-1/2}} \left\{ \frac{1}{\sqrt{\mu_L^3}} \frac{g_{2i}g_{2m}}{\tau_2} \delta(t - \tau_2) + \frac{1}{\mu_T \sqrt{\mu_L}} \frac{g_{3i}g_{3m}}{\tau_3} \delta(t - \tau_3) \right\}, \quad (3.11)$$

where

$$\begin{cases} \mathbf{g}_2 = \frac{-1}{\sqrt{\gamma_1^2 + \gamma_2^2}}(-\gamma_2\gamma_3, -\gamma_2\gamma_3, \gamma_1^2 + \gamma_2^2) \\ \mathbf{g}_3 = \frac{1}{\sqrt{\gamma_1^2 + \gamma_2^2}}(\gamma_2, -\gamma_1) \end{cases}, \tag{3.12}$$

and

$$\begin{cases} \tau_2 = \frac{r}{\sqrt{\mu_L/\rho}} \\ \tau_3 = \frac{r}{\sqrt{\mu_T/\rho}} \sqrt{\gamma_1^2 + \gamma_2^2 + \frac{\mu_T}{\mu_L}\gamma_3^2} \end{cases}. \tag{3.13}$$

Using Eq. (3.11), the displacement field induced by the moving point force for the case of $C = 0$ can be derived. The key results are given below, and the derivations can be found in SI3.

For a TI solid, without loss of generality, we let the moving direction of source \mathbf{a} lie in the $x_1 - x_3$ plane and let α be the angle between the x_3 -axis and \mathbf{a} , so that $\mathbf{a} = (-\sin \alpha, 0, \cos \alpha)$, as shown in Fig. 4b. The two transverse wave modes, SH and qSV, correspond to two successive terms on the right hand side of Eq. (3.11). By separating the resulting displacements into two parts, $u_i = u_i^{qSV} + u_i^{SH}$, we have

$$u_i^{qSV} = \frac{1}{\sqrt{1 - M_{qSV}^2 \sin^2 \theta(t)}} F^{qSV}(\mathbf{x}, t, \tau_1^{qSV}, \tau_2^{qSV}), \tag{3.14}$$

where $M_{qSV} = v_e/v_{qSV}$, and $v_{qSV} = \sqrt{\mu_L/\rho}$, according to Eq. (2.11), when $C = 0$,

$$\tau_{1,2}^{qSV} = t + \frac{R(t)}{(M_{qSV}^2 - 1)\sqrt{\mu_L/\rho}} \left(M_{qSV} \cos \theta(t) \pm \sqrt{1 - M_{qSV}^2 \sin^2 \theta(t)} \right), \tag{3.15}$$

and the definitions of $\mathbf{R}(t)$ and $\theta(t)$ are given by Eq. (3.8).

Eq. (3.14) is basically in the same form as Eq. (3.5), as expected, because the phase velocity v_{qSV} and the group velocity for the qSV mode are independent of the spatial direction for $C = 0$.

For the SH mode, the phase velocity v_{SH} varies with the spatial direction; in this case, the resulting Mach cone is no longer a perfect cone (Fig. 4b). To make the expression of the resulting displacement more concise and consistent with Eq. (3.5) or Eq. (3.14), we introduce the coordinate transformation

$$\begin{cases} x'_1 = x_1 \\ x'_2 = x_2 \\ x'_3 = \beta x_3 \end{cases}, \tag{3.16}$$

where $\beta^2 = \frac{\mu_T}{\mu_L}$ is a dimensionless parameter that gives a measure of the anisotropic properties of the material. When $C = 0$ and $\beta = 1$, the material is isotropic, whereas when $C \neq 0$ and $\beta = 1$, the phase velocities of the SH mode do not vary with the spatial direction based on Eq. (2.9), although the material may be anisotropic. In the new coordinate system, the speed v'_e of the moving source is

$$v'_e = v_e \sqrt{\sin^2 \alpha + \beta^2 \cos^2 \alpha}, \tag{3.17}$$

and the unit vector in the moving direction is

$$\mathbf{a}' = \frac{(\sin \alpha, 0, \beta \cos \alpha)}{\sqrt{\sin^2 \alpha + \beta^2 \cos^2 \alpha}}. \tag{3.18}$$

The resulting displacement for the SH mode in the transformed coordinate system is (see SI4 for details)

$$u_i^{SH} = \frac{1}{\sqrt{1 - M_{SH}^2 \sin^2 \theta_{SH}}} F^{SH}(\mathbf{x}', t, \tau_1^{SH}, \tau_2^{SH}), \tag{3.19}$$

where $M_{SH} = v'_e/\sqrt{\mu_T/\rho}$ is defined as the Mach number,

$$\tau_{1,2}^{SH} = t + \frac{R'}{\sqrt{\mu_T/\rho}(M_{SH}^2 - 1)} \left(M_{SH} \cos \theta'(t) \pm \sqrt{1 - M_{SH}^2 \sin^2 \theta'(t)} \right), \tag{3.20}$$

and

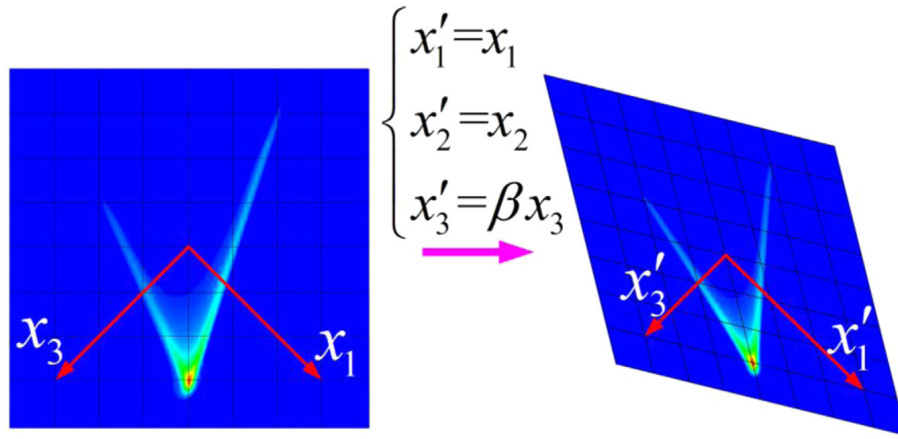


Fig. 5. In the transformed coordinate system, the displacement is confined in a Mach cone.

$$\begin{cases} \mathbf{R}'(t) = \mathbf{x}' - v_e t \mathbf{a}' \\ \cos \theta'(t) = \arccos\left(\frac{\mathbf{R}' \cdot \mathbf{a}'}{R'}\right) \end{cases} \quad (3.21)$$

Eq. (3.19) shows that the displacement is confined in a Mach cone in the transformed coordinate system, as illustrated in Fig. 5. This transformation provides a useful tool to study the profile of the wave fronts in an anisotropic soft medium generated by a moving source, e.g., the existence of the Mach cone and its cone angle. In the SSI technique (Bercoff et al., 2004a), the source moves with supersonic speed, and the Mach number is very large. Thus, our analytical results given by Eq. (3.19) reveal that quasi-plane waves can be generated. The speed of the wave fronts along the direction of the wave vector can be measured experimentally by relying on the time-of-flight algorithm (McLaughlin and Renzi, 2006; Tanter et al., 2008), which can be combined with Eq. (2.9) to further infer the elastic properties of anisotropic soft materials.

The analytical solution was derived here under the condition of $C = 0$. Fig. 3 illustrates that parameter C plays an important role in determining the spatial variation of the shear wave velocity. We now investigate the ECE in more general cases with $C \neq 0$.

4. Computational studies on the ECE in an incompressible TI solid

For incompressible TI solids with $C \neq 0$, it is difficult to obtain the solutions in analytical forms similar to Eqs. (3.14) and (3.19). In this section, we use finite element analysis (FEA) to study the ECE in more general cases.

The FEA is conducted using the commercial software Abaqus/explicit (2010). A cubic solid of size $40 \text{ mm} \times 40 \text{ mm} \times 40 \text{ mm}$ is used to model the soft media. The model contains 4,096,000 C3D8R elements. Following previous treatments of acoustic radiation force (ARF) (Palmeri et al., 2005; Rouze et al., 2013), the moving source is modeled as the following body force with a three-dimensional Gaussian distribution, traveling uniformly with speed v_e ,

$$f_i(\mathbf{x}, t) = a_i F_0 e^{-\frac{(\mathbf{x} - v_e t \mathbf{a})^2}{r_0^2}}, \quad (4.1)$$

where $F_0 = 10^{-3} \text{ N}$ denotes the amplitude of the force, the unit vector \mathbf{a} is along the movement direction, and $r_0 = 0.5 \text{ mm}$. We rely on the user subroutine of VLoad in Abaqus.

As mentioned in Section 2, the parameter C plays a key role in investigations of the ECE in a TI soft material. We divide incompressible TI solids into three classes: $C > 0$, $C = 0$ and $C < 0$. In our FEA, we consider three different TI materials, with representative material constants given in Table 1.

We again choose a coordinate system such that the x_3 -axis is parallel to the fibers. The source moves in a line making an angle α with the fibers, so that $\mathbf{a} = (-\sin \alpha, 0, \cos \alpha)$. We investigate the following three different cases in turn:

Table 1
Elastic parameters used in the FE simulations.

	E_L (kPa)	μ_L (kPa)	μ_T (kPa)
$C = 62.5 \text{ kPa}$	216	25	9
$C = 0$	91	25	9
$C = -21.875 \text{ kPa}$	47.25	25	9

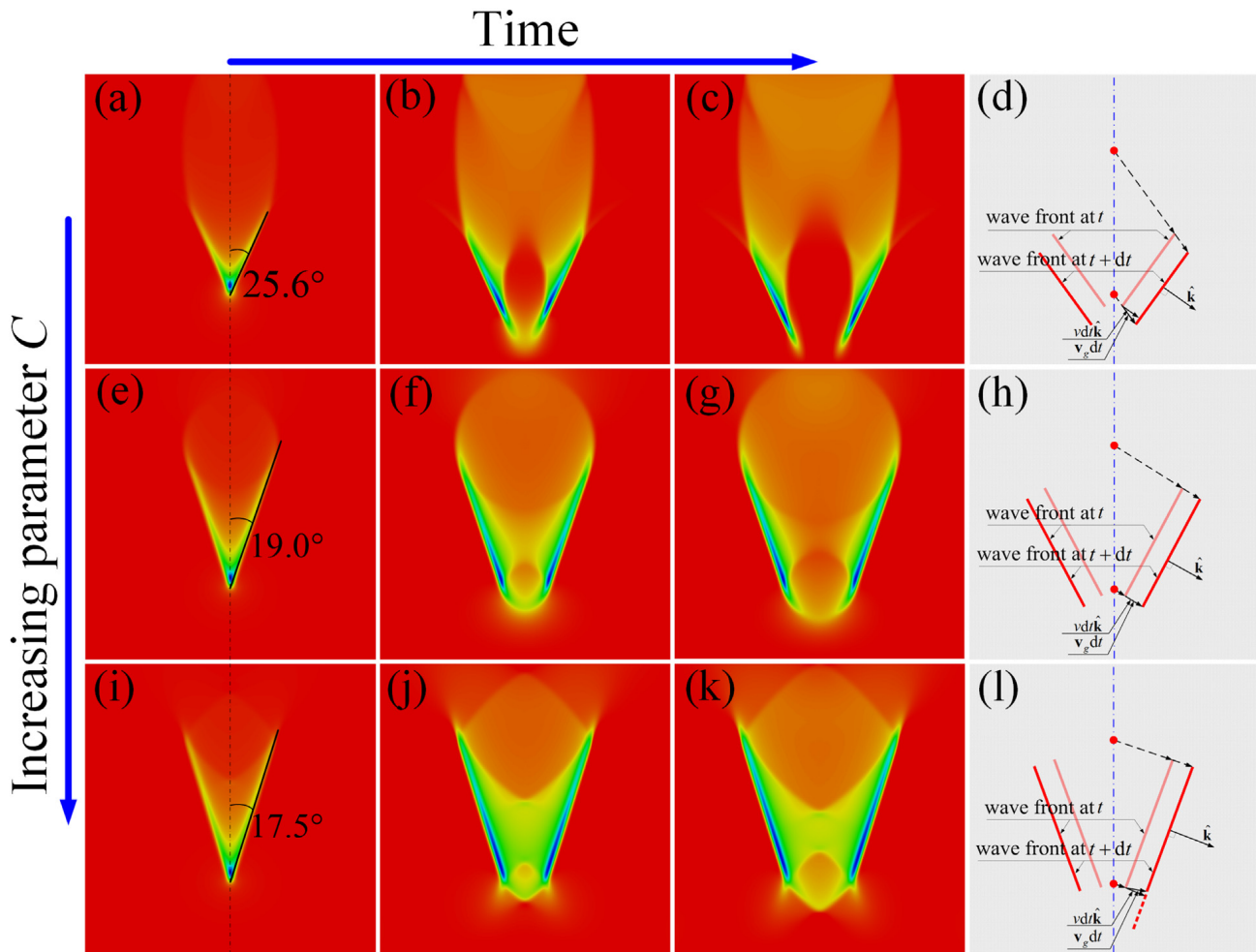


Fig. 6. The ECE at low Mach number when the force is moving along the material symmetric axis direction. The angles of the Mach cones are (a) 25.6°, (e) 19.0°, (i) 17.5°. (a)–(c) for $C > 0$, (e)–(g) for $C = 0$ and (i)–(k) for $C < 0$. In general, the wave vectors are not in the same direction as the group velocities, except when $C = 0$. The phase velocities are the projections of the group velocities in the directions of the wave vectors, as schematically given by (d), (h) and (l).

$$\alpha = 0^\circ, 90^\circ, 45^\circ.$$

4.1. Source moving along the fibers $\alpha = 0^\circ$

When the source moves along the direction $\alpha = 0^\circ$, the problem is axisymmetric. In this case, the shear wave of the qSV mode is the main concern, and its speed can be measured with the SSI technique.

We first study the case where the Mach number, $M_{qSV} = v_e / \sqrt{\mu_L / \rho}$, is relatively small to reveal the key features of the ECE in an anisotropic soft medium. The source speed is taken as $v_e = 15\text{m/s}$ in our simulations, which corresponds to $M_{qSV} = 3$. The representative results shown in Fig. 6 indicate that the resulting shear-wave Mach cones depend strongly on parameter C . For instance, for $C > 0$ (Fig. 6a–d), we first measure the angle of the Mach cone (Fig. 6a) based on the FE results. Then, inserting the wave vector of $\hat{\mathbf{k}} = (\sin \theta, 0, \cos \theta)$ into Eq. (2.11) (so that the angle of the Mach cone is $(90^\circ - \theta)$) and using the geometric condition $v_{qSV}/v_e = \sin(90^\circ - \theta)$, we have

$$\frac{\sqrt{(\mu_L + 2C \sin^2 \theta \cos^2 \theta) / \rho}}{v_e} = \sin(90^\circ - \theta). \quad (4.2)$$

Solving Eq. (4.2) with the material parameters given by the first line in Table 1 results in $(90^\circ - \theta) \approx 25.5^\circ$, which is in good agreement with the value obtained from the FE simulations (Fig. 6a).

Fig. 6 shows that the shear-wave Mach cones are dependent on parameter C (or the elastic parameter E_L), and in this sense, it is theoretically possible to evaluate the elastic parameter E_L by measuring the angle of the Mach cone. However, our analysis shows that the variation of the cone angle is not sensitive to the variation in E_L , thus indicating that the solution to the inverse problem will be very sensitive to data errors.

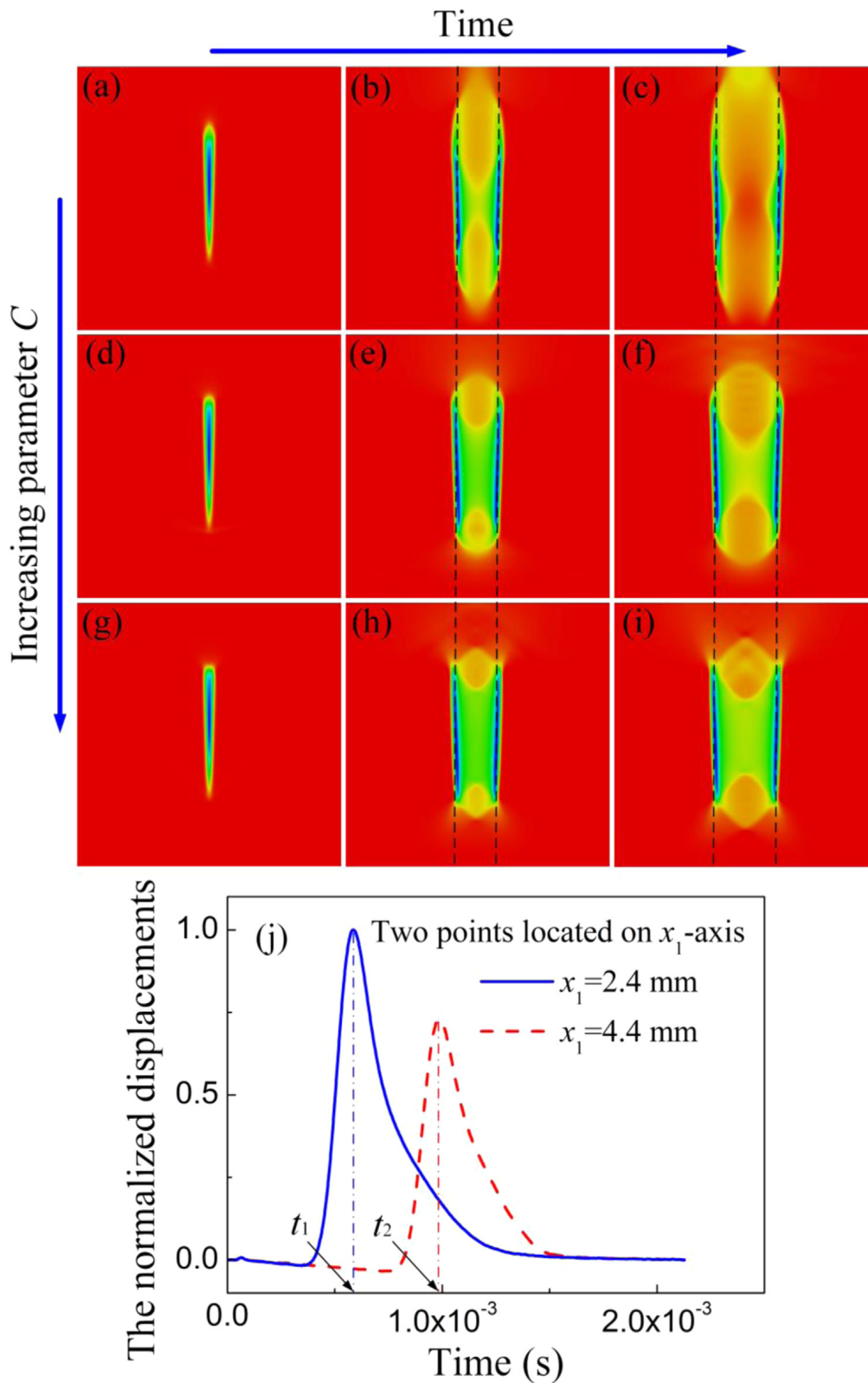


Fig. 7. The ECE at high Mach number when the force is moving along the material symmetric axis direction. (a)-(c) for $C > 0$, (d)-(f) for $C=0$, (g)-(i) for $C < 0$. The angle of the Mach cone is approximately equal to zero, and quasi-plane waves are formed. (j) The normalized displacements of two points located on the x_1 -axis are plotted, from which the velocity of the shear wave can be determined.

Fig. 6 also shows that the direction of the wave vector $\hat{\mathbf{k}}$ is not always consistent with the direction of the group velocity \mathbf{v}_g , as expected for wave motion in an anisotropic medium (Thomsen, 1986). A schematic of this phenomenon is given in Fig. 6.

For all three cases in Table 1, the movement distances of the source are the same, but the interfered wave fronts are different, simply because the directions of the group velocities are not the same (see Fig. 6d, h and l). In general, the interfered wave fronts in anisotropic media travel along the directions of the group velocities, which usually differ from the directions of the wave vectors, except in some special cases (e.g., $C = 0$ in the present problem).

We then investigate the case in which the Mach number is large. In experiments (Bercoff et al., 2004b), the source can move at supersonic speed, and the Mach number can be very large (~ 1000). We can see from Eq. (4.2) that the angle of the Mach cone, $(90^\circ - \theta)$, is close to zero when $M_{qSV} = v_e/\sqrt{\mu_L/\rho}$ is large. In our FEA model, we take $M_{qSV} = 30$. Fig. 7a, d and g show that the resulting angles of the Mach cone for all three cases are very close to zero, i.e., $\theta \approx 90^\circ$. In this case, the wave vector is almost aligned with x_1 : $\hat{\mathbf{k}} = (1, 0, 0)$. In practical experiments, the wave speed $v_{qSV,\perp}$ along the direction of the wave vector is measured, and the phase velocity formula (Eq. (2.11)) can be simply used to determine μ_L

$$\rho v_{qSV,\perp}^2 = \mu_L, \tag{4.3}$$

where the subscript ‘ \perp ’ denotes that the propagation direction of the shear wave is perpendicular to the fibers. In our analysis, the parameter μ_L is taken as constant in all three cases; therefore, the phase velocities of the shear waves should also have the same values (Fig. 7).

We also plot the normalized displacements in Fig. 7j for two points located along the direction of the wave vector (i.e., along the x_2 -axis). Then, by tracking the time delay of the peaks on the curves, we can calculate the speed of the shear wave $v_{qSV,\perp}$.

4.2. Source moving perpendicular to the fibers $\alpha = 90^\circ$

In this case, only the SH modes exist in the ultrasound imaging plane, according to the discussion in Section 2. The Mach number is $M_{SH} = v'_e/\sqrt{\mu_T/\rho}$, where v'_e defined in Eq. (3.17) is v_e when $\alpha = 90^\circ$. In our simulations, we took $M_{SH} = 50$. The

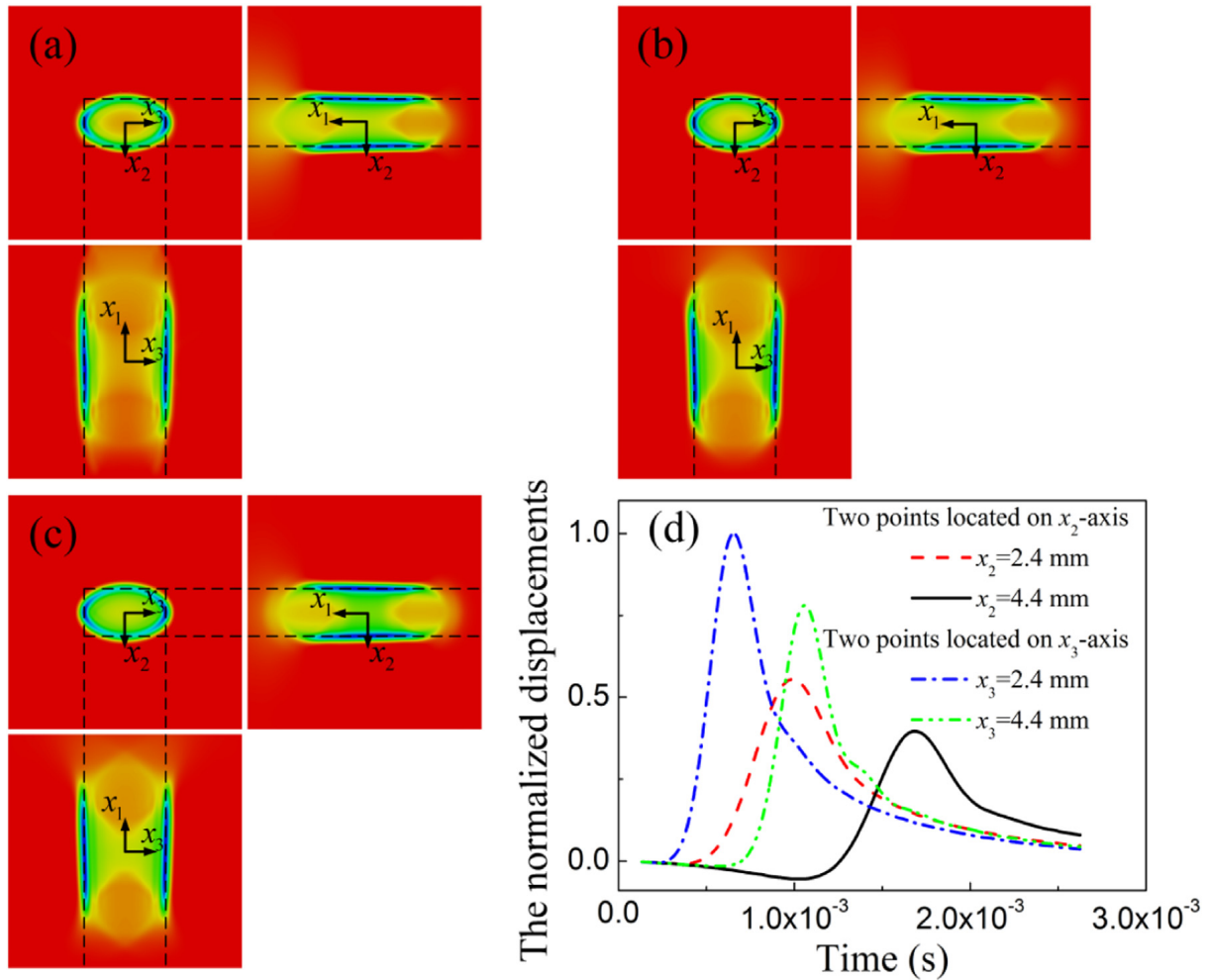


Fig. 8. The ECE at a high Mach number when the shear source is moving perpendicular to the material symmetric axis. (a) for $C > 0$, (b) $C=0$, (c) $C < 0$. (d) The normalized displacements for two points located on x_2 -axis and two points located on x_3 -axis are plotted to calculate $v_{SH,\perp}$ and $v_{SH,\parallel}$.

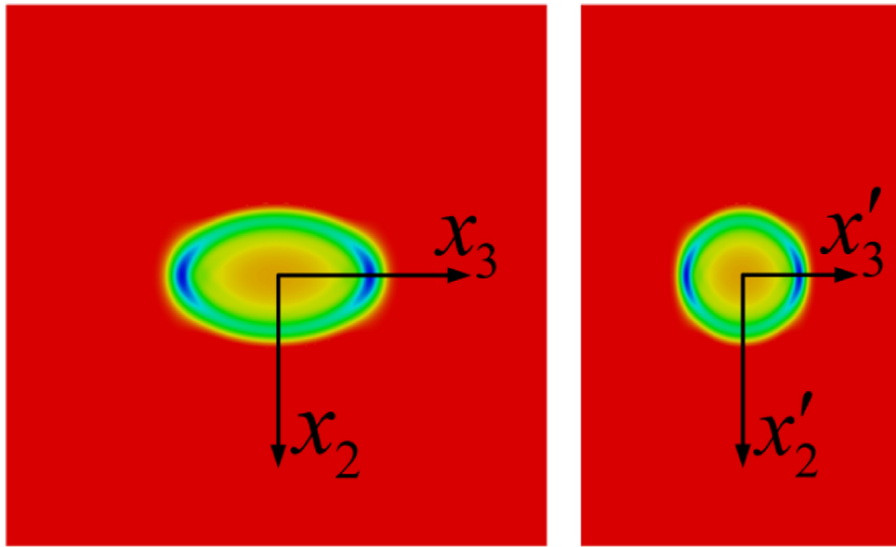


Fig. 9. The Mach cones in the original and transformed coordinate systems according to the FE results.

results in Fig. 8a-c show that the resulting shear waves are basically the same, even though the elastic parameter C (or E_L) is different in all three cases, thus confirming the analytical result that the SH mode is dependent on only μ_L and μ_T , as described in Section 3. In our FEA, the parameters μ_L and μ_T are fixed according to Table 1, thus explaining why the speeds of the resulting waves for the three cases are essentially the same. The shear wave speeds $v_{SH,\perp}$ and $v_{SH,\parallel}$ that are perpendicular to and along the fibers, respectively, are determined from the variation of the displacements with time at four characteristic points, as plotted in Fig. 8d. Given that the quasi-plane waves are generated at a high Mach number, the correlations between the phase velocities and the shear moduli perpendicular to and along the fibers are given by (Thomsen, 1986)

$$\begin{cases} \rho v_{SH,\perp}^2 = \mu_T \\ \rho v_{SH,\parallel}^2 = \mu_L \end{cases} \quad (4.4)$$

A number of authors have combined Eq. (4.4) and the SSI technique (Gennisson et al., 2010; Lee et al., 2012) to determine μ_L and μ_T for an incompressible TI soft tissue. Our above analysis shows that Eq. (4.4) is applicable, provided that the movement speed of the source is high, and thus, the Mach number is large, and quasi-plane waves are generated.

In Section 3, we introduced a transformation of coordinates to obtain the Mach cone of the SH mode in the form of a perfectly circular cone. As a further illustration, the Mach cones in the original coordinate system and that in the transformed coordinate system are compared in Fig. 9, taking $C = 62.5$ kPa as an example. Clearly, in the transformed coordinate system, a Mach cone in the form of a circular cone is achieved.

4.3. Source moving oblique to the fibers $\alpha = 45^\circ$

The analysis above shows that in the cases of $\alpha = 90^\circ$ and $\alpha = 0^\circ$, shear-wave Mach cones and quasi-plane waves can be generated by the moving shear source, which provides a reliable means to determine the initial shear moduli μ_L and μ_T from the wave velocities simply by using Eq. (4.4) (for both μ_L and μ_T) or Eq. (4.3) (for μ_L). However, determining the third elastic parameter E_L remains challenging. Bearing this important issue in mind, we investigate the case in which the angle between the movement direction of the source and the material symmetric axis is 45° (Fig. 2c), inspired by the recent study by Rouze et al. (2013) on ARF impulse (ARFI) elastography. In this case, the qSV mode may be used to access the parameter E_L .

Fig. 10 gives the computational results. Clearly, the resulting shear-wave Mach cones are significantly different from those observed in the cases of $\alpha = 90^\circ$ and $\alpha = 0^\circ$, and they strongly depend on parameter C (or E_L). When $C > 0$ (Fig. 10g), two shear waves with different polarization directions are clearly observed, in contrast to when $C \leq 0$ (Fig. 10h and i). This result may be explained as follows. When $C > 0$, two wave modes are excited, and they have different speeds on the ultrasound imaging plane, as illustrated in Fig. 10d. Then, Eq. (2.11) and the definition of parameter C indicate that the phase velocity of the qSV mode is greater than that of the other mode. When $C \leq 0$, the displacements generated by the source moving at a high speed will be approximately parallel to the loading direction, and therefore, only the qSV mode can be observed on the ultrasound imaging plane, as shown in Fig. 10e and f. In summary, the interfered wave fronts tracked in experiments using the SSI technique (Bercoff et al., 2004a) will always be the qSV modes when $\alpha = 45^\circ$. The normalized displacements of two characteristic points located along the direction of wave vector are plotted in Fig. 10g–i, enabling evaluation of the speeds of the quasi-plane shear waves. Furthermore, the following correlation between the phase velocity of the qSV mode and the material parameters may be used to establish an inverse approach to measure parameter C (or E_L),

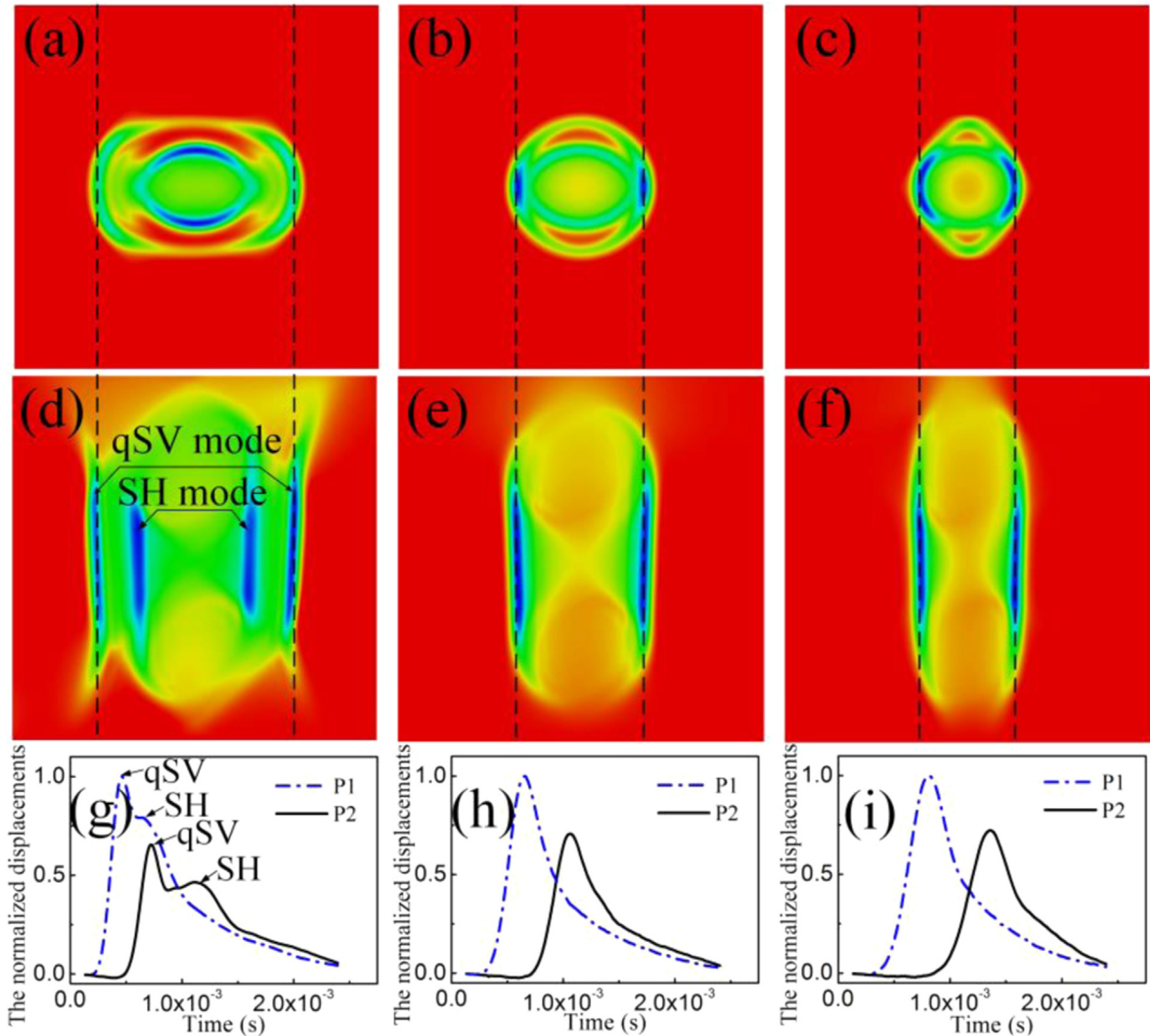


Fig. 10. The ECE at a high Mach number when the angle between the direction of the moving force and the material symmetric axis is taken as $\alpha = 45^\circ$, (a), (d) and (g) for $C > 0$; (b), (e) and (h) for $C = 0$; (c), (f) and (i) for $C < 0$.

as shown in detail in Section 6.

$$\rho v_{qSV,45^\circ}^2 = \mu_L + C/2. \quad (4.5)$$

5. Propagation of shear waves in a deformed anisotropic soft material

In the previous sections, we investigated the ECE in an incompressible and stress-free TI material. The results may be used together with the dynamic elastography method, e.g., the SSI technique (Bercoff et al., 2004a), to determine the anisotropic elastic parameters of biological soft tissues. Notably, (a) in clinical use, contact between the probe and the tissue may lead to finite deformation in the soft tissue and (b) knowing how shear waves propagate in a deformed soft tissue (the theory of acousto-elasticity) can facilitate understanding of its hyperelastic (nonlinear elastic) properties (Gennisson et al., 2007; Rénier et al., 2008; Latorre-Ossa et al., 2012; Jiang et al., 2015a; 2015b). In this section, we thus investigate the propagation of shear waves in a deformed incompressible TI soft medium.

The theory of elastic wave propagation in deformed solids dates back to the works of Hadamard (1903), Brillouin (1925) and Biot (1940). This theory was later rewritten in compact form by Ogden and collaborators (see Ogden (2007) for a review

or Ogden and Singh (2011)) and was further developed within the framework of finite elasticity. Here, we rely on these equations to derive analytical solutions predicting the speed of the shear waves generated in an incompressible anisotropic soft tissue by a moving source. In our derivations, we use the constitutive relationship proposed by Murphy (2013) because it is compatible with the linear elastic TI model with infinitesimal deformation and motion. This provides a strong link to the ultrasonic measurements made on un-deformed solids; however, any other hyperelastic model could be used in our analysis.

5.1. Governing equations

Here, we briefly recall the governing equations used to analyze the propagation of homogeneous shear waves in a deformed hyperelastic solid (see Ogden (2007) for more details).

We consider small-amplitude motions in an incompressible TI material with a strain energy density W that has been subjected to a large homogeneous deformation described by the constant deformation gradient $\mathbf{F} = \partial\mathbf{x}/\partial\mathbf{X}$, where \mathbf{x} and \mathbf{X} are the spatial and material coordinates, respectively. The displacement $\mathbf{u}(\mathbf{x}, t)$ satisfies the following incremental equations of motion and the condition of incompressibility (Ogden, 2007)

$$\begin{cases} A_{0piqj}u_{j,qp} - \delta p_{,i} = \rho u_{i,tt} \\ u_{i,i} = 0 \end{cases}, \quad (5.1)$$

where δp is the increment of the Lagrange multiplier p due to the internal constraint of incompressibility, and \mathbf{A}_0 is the fourth-order tensor of the instantaneous elastic moduli, with components

$$A_{0piqj} = F_{pa}F_{q\beta} \frac{\partial^2 W}{\partial F_{ia} \partial j\beta}. \quad (5.2)$$

5.2. Constitutive relation

Several constitutive models have been proposed over the years to characterize incompressible TI soft tissues (e.g., Humphrey and Yin, 1987; Merodio and Ogden 2003, 2005; Destrade et al., 2013; Murphy, 2013). In general, their strain-energy function W may be written as a function of four invariants,

$$W = W(I_1, I_2, I_4, I_5), \quad (5.3)$$

where $I_1 = \text{tr}(\mathbf{C})$, $I_2 = \frac{1}{2}[\text{tr}(\mathbf{C})^2 - \text{tr}(\mathbf{C}^2)]$ are the isotropic invariants, $\mathbf{C} = \mathbf{F}^T\mathbf{F}$ is the right Cauchy-Green deformation tensor, and I_4 and I_5 are the anisotropic invariants,

$$I_4 = \mathbf{M} \cdot \mathbf{C} \mathbf{M}, \quad I_5 = \mathbf{M} \cdot \mathbf{C}^2 \mathbf{M}. \quad (5.4)$$

Here, the unit vector \mathbf{M} is along the fibers, which we chose to be aligned with the x_3 -axis of the coordinate system, so that $\mathbf{M} = (0, 0, 1)$.

The corresponding Cauchy stress tensor is (Spencer, 1972)

$$\begin{aligned} \boldsymbol{\sigma} = & -p\mathbf{I} + 2W_1\mathbf{B} + 2W_2(I_1\mathbf{B} - \mathbf{B}^2) + 2W_4\mathbf{F}\mathbf{M} \otimes \mathbf{F}\mathbf{M} \\ & + 2W_5(\mathbf{F}\mathbf{M} \otimes \mathbf{B}\mathbf{F}\mathbf{M} + \mathbf{B}\mathbf{F}\mathbf{M} \otimes \mathbf{F}\mathbf{M}), \end{aligned} \quad (5.5)$$

where $\mathbf{B} = \mathbf{F}\mathbf{F}^T$ is the left Cauchy-Green deformation tensor, and $W_i = \frac{\partial W}{\partial I_i}$ ($i \in \{1, 2, 4, 5\}$). When the material is undeformed ($\mathbf{F} = \mathbf{I}$) and stress free,

$$\begin{cases} p^0 = 2W_1^0 + 4W_2^0 \\ W_4^0 + 2W_5^0 = 0 \end{cases}, \quad (5.6)$$

where the superscript 0 indicates that the quantities are evaluated at the ground state, where $I_1 = I_2 = 3$, $I_4 = I_5 = 1$.

For infinitesimal deformations, three independent elastic parameters, i.e., μ_T , μ_L and E_L , are required to describe the mechanical behavior of the incompressible TI solid, as noted earlier. Merodio and Ogden (2003, 2005) have presented the conditions to ensure the compatibility between the linear elastic and hyperelastic models, which can be written as (Murphy, 2013)

$$\begin{cases} 2W_1^0 + 2W_2^0 = \mu_T \\ 2W_1^0 + 2W_2^0 + 2W_5^0 = \mu_L \\ 4W_{44}^0 + 16W_{45}^0 + 16W_{55}^0 = E_L + \mu_T - 4\mu_L \end{cases}, \quad (5.7)$$

where W_{ij} is $\partial^2 W / \partial I_i \partial I_j$ ($i, j \in \{1, 2, 4, 5\}$).

Murphy (2013) has noted that W should include both I_4 and I_5 to meet the initial condition given by Eq. (5.7). Furthermore, the strain-energy function may be written in the following form:

$$W = \mathcal{F}(I_1, I_4) + \frac{\mu_T - \mu_L}{2}(2I_4 - I_5 - 1). \tag{5.8}$$

Eq. (5.8) is compatible with the linear elastic model. Bearing Eq. (5.8) in mind, Murphy (2013) has generalized the material model proposed by Humphrey-Yin (1987) to the following form, which is used in this study

$$W = \frac{\mu_T}{2c_2} [e^{c_2(I_1-3)} - 1] + \frac{E_L + \mu_T - 4\mu_L}{2c_4} [e^{c_4(I_4^{1/2}-1)^2} - 1] + \frac{\mu_T - \mu_L}{2}(2I_4 - I_5 - 1). \tag{5.9}$$

where $c_2 > 0$ and $c_4 > 0$ are the isotropic and anisotropic strain-hardening parameters, respectively, and $I_4 = \mathbf{M} \cdot \mathbf{C} \mathbf{M}$ is the squared stretch in the direction of the fibers. To simplify these expressions, we will use A , B and C to denote $\frac{\mu_T}{2}$, $\frac{\mu_T - \mu_L}{2}$ and $\frac{E_L + \mu_T - 4\mu_L}{2}$, respectively. Importantly, when the parameter $C=0$, the effect of the hardening parameter c_4 will not apply.

Using the strain-energy function Eq. (5.9), we can compute the elastic moduli explicitly as (e.g., see Destrade, 2015)

$$A_{0ijkl} = 2W_1 \delta_{il} B_{jk} + 2W_4 \delta_{il} m_j m_k + 2W_5 [\delta_{il} (\mathbf{B} \mathbf{m})_j m_k + \delta_{il} (\mathbf{B} \mathbf{m})_k m_j + B_{jk} m_i m_l + B_{ji} m_i m_k + B_{ik} m_j m_l + B_{il} m_j m_k] + 4W_{11} B_{ij} B_{kl} + 4W_{44} m_i m_j m_k m_l, \tag{5.10}$$

where $\mathbf{m} = \mathbf{B} \mathbf{M}$ and

$$W_1 = A e^{c_2(I_1-3)}, W_4 = 2B + C e^{c_4(I_4^{1/2}-1)^2} (1 - I_4^{-1/2}), W_5 = -B, \\ W_{11} = c_2 A e^{c_2(I_1-3)}, W_{44} = c_4 C e^{c_4(I_4^{1/2}-1)^2} (1 - I_4^{-1/2})^2 + \frac{1}{2} C e^{c_4(I_4^{1/2}-1)^2} I_4^{-3/2}. \tag{5.11}$$

5.3. An analytical solution to predict the speed of a shear wave in a deformed TI solid

In this subsection, an analytical solution is derived to predict the effects of a finite deformation in a soft material on the propagation of the SH wave (Fig. 2b). In Sections 3 and 4, we showed the presence of the ECE and the quasi-plane waves generated at a high Mach number. Therefore, in this section, we consider the propagation of the plane waves of the form (Destrade et al., 2010a, 2010b)

$$\begin{cases} \mathbf{u} = \mathbf{U} e^{ik(\hat{\mathbf{k}} \cdot \mathbf{x} - vt)} \\ \delta p = ik P e^{ik(\hat{\mathbf{k}} \cdot \mathbf{x} - vt)} \end{cases}, \tag{5.12}$$

where \mathbf{U} is the amplitude of the wave (without loss of generality, \mathbf{U} is taken as a unit vector), $\hat{\mathbf{k}}$ is the unit vector in the direction of wave propagation, k is the wave number, v is the phase velocity, and P is a scalar.

Inserting \mathbf{u} and δp into the incremental equations of equilibrium Eq. (5.1) gives

$$\mathbf{Q}(\hat{\mathbf{k}}) \mathbf{U} - P \hat{\mathbf{k}} = \rho v^2 \mathbf{U}, \tag{5.13}$$

where $[Q(\hat{\mathbf{k}})]_{ij} = A_{0piqj} \hat{k}_p \hat{k}_q$ is the acoustic tensor. The constraint of incremental incompressibility given in Eq. (5.1) becomes

$$\mathbf{U} \cdot \hat{\mathbf{k}} = 0, \tag{5.14}$$

which means that the wave is purely transverse. Taking the dot product of Eq. (5.13) with $\hat{\mathbf{k}}$ gives

$$P = \hat{\mathbf{k}} \cdot \mathbf{Q}(\hat{\mathbf{k}}) \mathbf{U}. \tag{5.15}$$

Inserting Eqs. (5.15) and (5.14) into Eq. (5.13), we arrive at the following symmetric eigenvalue problem

$$(\mathbf{I} - \hat{\mathbf{k}} \otimes \hat{\mathbf{k}}) \mathbf{Q}(\hat{\mathbf{k}}) (\mathbf{I} - \hat{\mathbf{k}} \otimes \hat{\mathbf{k}}) \mathbf{U} = \rho v^2 \mathbf{U}. \tag{5.16}$$

Taking the dot product of Eq. (5.13) with \mathbf{U} together with the expression of $[Q(\hat{\mathbf{k}})]_{ij}$ gives the expression of the wave speed

$$\rho v^2 = \mathbf{U} \cdot \mathbf{Q}(\hat{\mathbf{k}}) \mathbf{U} = A_{0piqj} \hat{k}_p \hat{k}_q U_i U_j. \tag{5.17}$$

Recall that x_3 is aligned with the fibers so that $\mathbf{M} = (0, 0, 1)$. We assume that the direction of the moving source is along x_2 , in line with the particulars of the SSI technique. In this case, the polarization direction of the SH wave is also along x_2 , i.e., $\mathbf{U} = (0, 1, 0)$. The direction of the wave propagation lies in the $x_1 - x_3$ plane and is given by, for example, $\hat{\mathbf{k}} = (\sin \theta, 0, \cos \theta)$.

As shown in Fig. 11, the homogeneous state of deformation in the region of interest can be described by

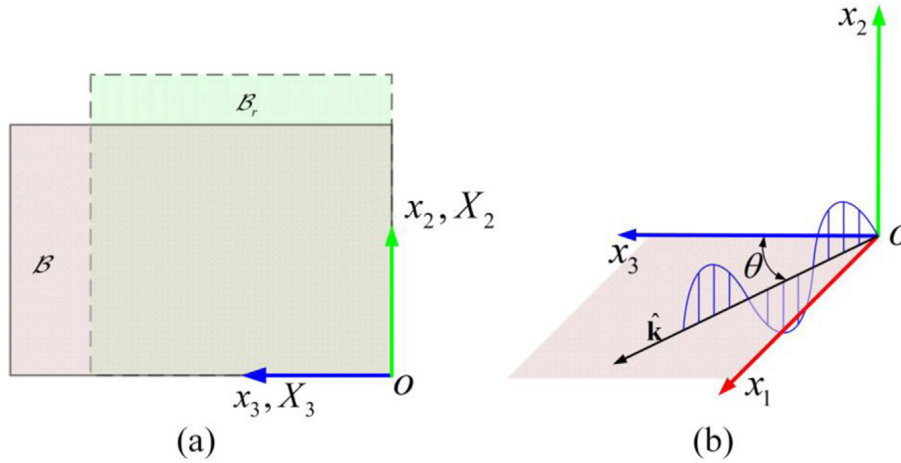


Fig. 11. (a) Illustration of the original and deformed configurations of the region of interest; (b) illustration of the wave vector.

$$\begin{cases} x_1 = \lambda_1 X_1 \\ x_2 = \lambda_2 X_2, \\ x_3 = \lambda_3 X_3 \end{cases} \tag{5.18}$$

where λ_1, λ_2 and λ_3 are the principal stretch ratios. The deformation gradient tensor \mathbf{F} corresponding to this deformation state is

$$\mathbf{F} = \lambda_1 \mathbf{e}_1 \otimes \mathbf{E}_1 + \lambda_2 \mathbf{e}_2 \otimes \mathbf{E}_2 + \lambda_3 \mathbf{e}_3 \otimes \mathbf{E}_3, \tag{5.19}$$

where \mathbf{e}_i and \mathbf{E}_α ($i, \alpha \in \{1, 2, 3\}$) are the base vectors of the material and spatial configurations, respectively. The constraint of incompressibility, $\det \mathbf{F} = 1$, yields $\lambda_1 \lambda_2 \lambda_3 = 1$. For the strain-energy function Eq. (5.9), the phase velocity v is determined from Eq. (5.17) as

$$\rho v^2 = 2Ae^{c_2(I_1-3)} \lambda_1^2 \sin^2 \theta + [2Ae^{c_2(I_1-3)} + 4B + 2Ce^{c_4(\lambda_3-1)^2} \left(1 - \frac{1}{\lambda_3}\right) - 2B(2\lambda_3^2 + \lambda_2^2)] \lambda_3^2 \cos^2 \theta, \tag{5.20}$$

where $I_1 = \lambda_1^2 + \lambda_2^2 + \lambda_3^2$.

Eq. (5.20) clearly shows how the shear wave speed depends on the material parameters and the deformation of the material. Based on Eq. (5.20), an inverse approach can be established to determine the constitutive parameters, as shown in Section 6 in detail. In the absence of deformation, $\lambda_1 = \lambda_2 = \lambda_3 = 1$, and Eq. (5.20) reduces to

$$\rho v^2 = \mu_T \sin^2 \theta + \mu_L \cos^2 \theta, \tag{5.21}$$

which is consistent with Eq. (2.9) when taking $\hat{\mathbf{k}} = (\sin \theta, 0, \cos \theta)$.

In the practical use of the SSI technique, the shear wave speeds in the directions along ($\theta = 0^\circ$) and perpendicular ($\theta = 90^\circ$) to the fibers are usually measured. After inserting $\theta = 90^\circ$ and $\theta = 0^\circ$ into Eq. (5.20), the speeds of the shear waves in these two directions are given by

$$\rho v_T^2 = 2Ae^{c_2(I_1-3)} \lambda_1^2, \tag{5.22}$$

$$\rho v_L^2 = \left[2Ae^{c_2(I_1-3)} + 4B + 2Ce^{c_4(\lambda_3-1)^2} \left(1 - \frac{1}{\lambda_3}\right) - 2B(2\lambda_3^2 + \lambda_2^2) \right] \lambda_3^2, \tag{5.23}$$

where v_L and v_T are the speeds along and perpendicular to the fibers, respectively.

To further illustrate the dependence of the shear wave speed given in Eqs. (5.22) and (5.23) on the deformation state, we now write $\lambda_2 = \lambda$ and $\lambda_1 = \lambda^{-\xi}$, so that $\lambda_3 = \lambda^{-(1-\xi)}$ because of the constraint of incompressibility. When compression is imposed along x_2 , the value of ξ should be in the range of $0.5 < \xi < 1$, with the lower bound corresponding to uni-axial compression/equi-biaxial deformation and the upper bound to plane strain deformation. Fig. 12 shows the variation of $\rho v_T^2/\mu_T$ and $\rho v_L^2/\mu_L$ with ξ for different λ . It can be seen that ξ exerts a significant influence only when λ is small for a propagation direction perpendicular to the fibers, e.g., $\lambda = 0.75$. This conclusion is consistent with that of Jiang et al. (2015a) for isotropic soft materials. However, when the propagation direction is along the material symmetric axis, $\rho v_L^2/\mu_L$ significantly depends on ξ , even when the deformation is small, e.g., $\lambda = 0.9$. Moreover, greater values of E_L correspond to more significant effects of ξ on $\rho v_L^2/\mu_L$. Our analytical solutions given by Eqs. (5.22) and (5.23) not only enable evaluation of the

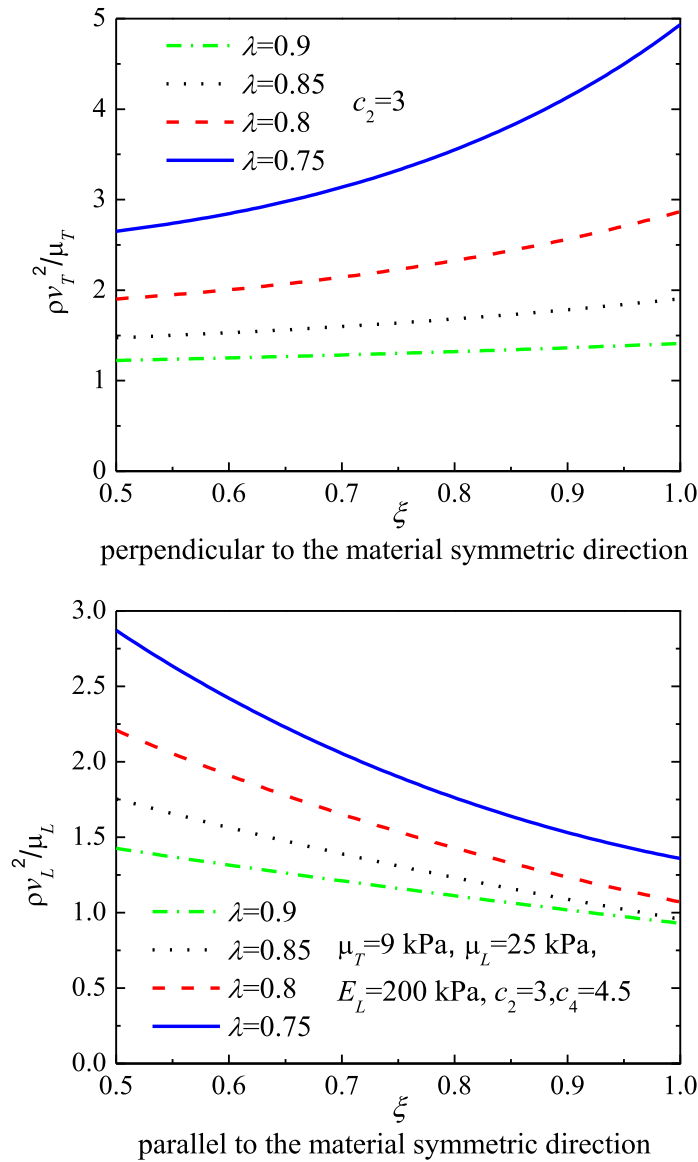


Fig. 12. Dependence of the shear wave velocities v_L and v_T on parameter ξ for different λ .

extent to which the deformation affects the wave velocities and the determination of the anisotropic parameters but also allow development of an inverse approach to determine the hyperelastic parameters of an incompressible TI soft material, as shown in detail in Section 6.

6. Inverse method to determine the linear and hyperelastic parameters of TI soft materials

In Sections 3–5, we investigated the ECE in a TI soft medium and the propagation of shear waves in a deformed material. Based on the theoretical and computational results, an inverse approach can be proposed to infer the anisotropic and hyperelastic parameters of an incompressible TI material.

6.1. Determination of anisotropic parameters μ_L , μ_T and E_L

Three elastic parameters, μ_L , μ_T and E_L , are required to describe a linear elastic incompressible TI soft material. The existence of the ECE in an anisotropic soft medium allows evaluation of μ_L and μ_T by using the correlation between the speed of the plane shear waves and the material parameters. Several authors have managed to measure μ_L and μ_T for skeletal muscles (Gennisson et al., 2010), skin (Luo et al., 2015), and kidneys (Gennisson et al., 2012) by using the SSI technique.

However, no effort has been made to infer the parameter E_L of soft tissues, which may be altered by injury or disease, by using the SSI technique. Our analysis in Section 4 shows that for $\alpha = 45^\circ$, quasi-plane waves can be formed when the Mach number is high, thus enabling determination of C or E_L by measuring the speed of the quasi-plane waves along the direction of $\hat{\mathbf{k}} = (\sin(\pi/4), 0, \cos(\pi/4))$, as denoted by $v_{qSV,45^\circ}$.

Based on Eq. (4.5), the elastic parameter C or E_L can be determined through the following relations:

$$\begin{aligned} C &= 2(\rho v_{qSV,45^\circ}^2 - \mu_L) \\ E_L &= 4\rho v_{qSV,45^\circ}^2 - \mu_T. \end{aligned} \quad (6.1)$$

6.2. Determination of the hyperelastic parameters c_2 and c_4

When the propagation direction of the shear wave is perpendicular to the fibers, we introduce the quantities λ and ξ and rewrite Eq. (5.22) as follows

$$\rho v_T^2 = 2Ae^{c_2(\lambda^2 + \lambda^{-2\xi} + \lambda^{-2(1-\xi)} - 3)} \lambda^{-2\xi}. \quad (6.2)$$

As explained previously, the transverse shear modulus μ_T can be determined from the measurements of v_T . Furthermore, the hardening parameter c_2 can be determined from the equation

$$c_2 = \frac{\ln\left(\frac{\rho v_T^2 \lambda^{2\xi}}{\mu_T}\right)}{\lambda^2 + \lambda^{-2\xi} + \lambda^{-2(1-\xi)} - 3}. \quad (6.3)$$

When the propagation direction of the shear wave is parallel to the fibers, Eq. (5.23) can be rewritten as follows:

$$\rho v_L^2 = [2Ae^{c_2(\lambda^2 + \lambda^{-2\xi} + \lambda^{-2(1-\xi)} - 3)} + 4B + 2Ce^{c_4(\lambda^{\xi-1} - 1)^2} (1 - \lambda^{1-\xi}) - 2B(2\lambda^{2\xi-2} + \lambda^2)] \lambda^{2\xi-2}, \quad (6.4)$$

In principle, parameter c_4 can be determined from Eq. (6.4) when parameter $C \neq 0$ as

$$c_4 = \frac{1}{(\lambda^{\xi-1} - 1)^2} \ln\left(\frac{\rho v_L^2 \lambda^{2\xi-2} - \mu_T e^{c_2(\lambda^2 + \lambda^{-2\xi} + \lambda^{-2(1-\xi)} - 3)} - (\mu_T - \mu_L)(2 - 2\lambda^{2\xi-2} - \lambda^2)}{(E_L + \mu_T - 4\mu_L)(1 - \lambda^{1-\xi})}\right). \quad (6.5)$$

It should be noted that in an *in vivo* measurement using the SSI technique, λ_3 is usually in the vicinity of 1, and therefore, parameter c_4 based on Eq. (6.5) will be very sensitive to data errors. However, in an *in vitro* or *ex vivo* measurement, a pre-deformation may be imposed along the fiber direction, and thus, c_4 may be obtained with good accuracy by using Eq. (6.5) and the SSI technique.

6.3. Properties of the solutions to the inverse problem

Determining the anisotropic and hyperelastic parameters of soft tissues from speed measurements is an inverse problem. The sensitivity of the identified solutions to data errors can be assessed by introducing the condition number. The condition number for the determination of μ_L , μ_T and E_L is 2, thus indicating that a 3% error in the measured wave velocity will lead to a 6% error in the identified solutions.

We then validate the inverse method by using numerical experiments. In Fig. 8d, we plot the normalized displacements of four characteristic points for $C = 62.5$ kPa. All of the points are located in the plane perpendicular to the movement direction of the shear source. Two points are located on the x_2 -axis (perpendicular to material symmetric axis), whereas the other two are located on the x_3 -axis. The distance between every two points is $\Delta d = 2.0$ mm. To measure the velocities of the shear waves, the time delays of the peaks on the curves, denoted by $\Delta t_{SH,\parallel}$ and $\Delta t_{SH,\perp}$, are measured. Then, the velocities can be calculated with $v_{SH,\perp} = \Delta d / \Delta t_{SH,\perp}$ and $v_{SH,\parallel} = \Delta d / \Delta t_{SH,\parallel}$, respectively. The time delay calculated by the FEA is shown in Fig. 8d, i.e., $\Delta t_{SH,\perp} = 0.69$ ms and $\Delta t_{SH,\parallel} = 0.40$ ms. Thus, we have $v_{SH,\perp} = 2.9$ m/s and $v_{SH,\parallel} = 5.0$ m/s. From Eq. (4.4), we deduce the material parameters μ_T and μ_L as $\mu_T = 8.4$ kPa and $\mu_L = 25.0$ kPa, respectively, results in good agreement with the input

Table 2

A comparison of the identified parameter C using Eq. (6.1) with those input in the numerical experiments.

Input C (kPa)	Time delay of the qSV mode (ms)	$v_{qSV,45^\circ}$ (m/s)	Identified C (kPa)
62.5	0.262	7.63	66.4
0	0.408	4.90	-1.98
-21.875	0.550	3.64	-23.5

parameters used in the FEA (Table 1).

In Fig. 10g-i, we plot the normalized displacements for P1 and P2 along the direction of the wave vector because they are also tracked in the SSI technique. From the figures, we obtain the time delays of the peaks on the curves. Furthermore, the shear wave speeds $v_{qSV,45^\circ}$ are calculated, and the parameters C are deduced according to Eq. (6.1). The results for the three cases are listed in Table 2. The parameters C (or E_L) deduced from the measured speeds match those input into the FEA well, thus indicating that our inverse approach is effective. The *in vivo* determination of the E_L of soft tissues using elastography remains challenging, but our method has great potential for practical use, as demonstrated in Part II of this paper.

In the determination of μ_T , μ_L and E_L , the deformation of soft tissues caused by contact with the ultrasound probe may lead to errors. Our analytical solutions given by Eqs. (5.22) and (5.23) allow quantitative estimation of the effects of the soft tissue deformation. For instance, in the determination of μ_T , if we take the hardening parameter $c_2 = 3$ as an example, then a deformation of $\lambda = 0.8$ may lead to an error up to 100% in the measured μ_T . Thus, the analytical solutions proposed here provide guidelines for controlling the effects of deformation on the measurement of anisotropic parameters by using the SSI technique.

The condition numbers that measure the sensitivity of the isotropic strain-hardening parameter c_2 and anisotropic parameter c_4 to the errors in $\rho v_T^2/\mu_T$ and $\rho v_L^2/\mu_L$ in analytical form are given by

$$\text{Cond}_{c_2} = \frac{\Delta c_2}{c_2} \frac{\Delta(\rho v_T^2/\mu_T)}{\rho v_T^2/\mu_T} = \frac{\rho v_T^2/\mu_T}{c_2} \frac{\partial c_2}{\partial(\rho v_T^2/\mu_T)} = \frac{1}{c_2(\lambda^2 + \lambda^{-2\xi} + \lambda^{-2(1-\xi)} - 3)} \quad (6.6)$$

and

$$\begin{aligned} \text{Cond}_{c_4} &= \frac{\Delta c_4}{c_4} \frac{\Delta(\rho v_L^2/\mu_L)}{\rho v_L^2/\mu_L} = \frac{\rho v_L^2/\mu_L}{c_4} \frac{\partial c_4}{\partial(\rho v_L^2/\mu_L)} \\ &= \frac{1}{\lambda_3(\lambda_3 - 1)^3 e^{c_4(\lambda_3 - 1)^2} C/\mu_L} \end{aligned} \quad (6.7)$$

respectively. Fig. 13 plots of the condition numbers according to Eqs. (6.6) and (6.7), which show that parameter λ plays an important role.

To obtain a more reliable evaluation of parameter c_2 , a smaller λ (larger deformation) should be used in practical measurements. Interestingly, Eq. (6.7) reveals that the stability of the identified c_4 depends only on λ_3 , in addition to the material parameters, regardless of the deformation state. In this sense, to obtain a reliable evaluation of c_4 , $\|\lambda_3 - 1\|$ should be sufficiently large. Moreover, Eq. (6.7) and Fig. 13 indicate that the identified c_4 may be sensitive to data errors for a material with a small C/μ_L ratio.

7. Concluding remarks

When a source is moving at a high speed (e.g., supersonic speed), shear-wave Mach cones may be formed and quasi-plane waves may be generated in a soft medium. This phenomenon is termed the ECE and has been studied in isotropic soft solids, thus forming the theoretical basis of the SSI method (Bercoff et al., 2004a, 2004b). In this paper, we investigated the ECE in an incompressible TI solid for the first time because many soft tissues belong to this class of materials. In summary, the following key results were obtained in Part I of the paper.

First, both a theoretical analysis and computational studies were performed to elucidate the salient feature of the ECE in an incompressible TI solid. Our results clearly demonstrate that the shear-wave Mach cones are generated by the moving source and quasi-plane waves are formed at high Mach numbers. These results have not been reported in previous studies and form the theoretical basis for the use of the SSI technique to characterize the TI soft tissues. In particular, over the past several decades, a number of analytical solutions have been proposed to predict the speeds of plane shear waves for different types of anisotropic solids (Carcione, 2007). These analytical solutions, together with the existence of the ECE and its salient features, as revealed in this paper, enable simple correlations between the shear wave speed and the material parameters to be obtained. These results show that not only μ_T and μ_L but also E_L may be determined from simple relations.

Second, we investigated the propagation of a shear wave in a deformed incompressible TI soft medium. On the basis of the theory proposed by Ogden (2007) and a constitutive model presented by Murphy (2013), we derived analytical solutions revealing the correlation among the shear wave speeds, material parameters and the deformation of the solid.

Third, based on the theoretical solutions presented above, we proposed an inverse approach to determine the anisotropic and hyperelastic parameters of an incompressible TI soft material. We showed that the initial shear moduli μ_T and μ_L , the elastic modulus E_L and the hyperelastic parameters c_2 and c_4 can be determined with our inverse approach.

Finally, we performed both a theoretical analysis and numerical experiments to investigate the properties of the solutions to the present inverse problem. Our theoretical analysis, in which the concept of the condition number is introduced,

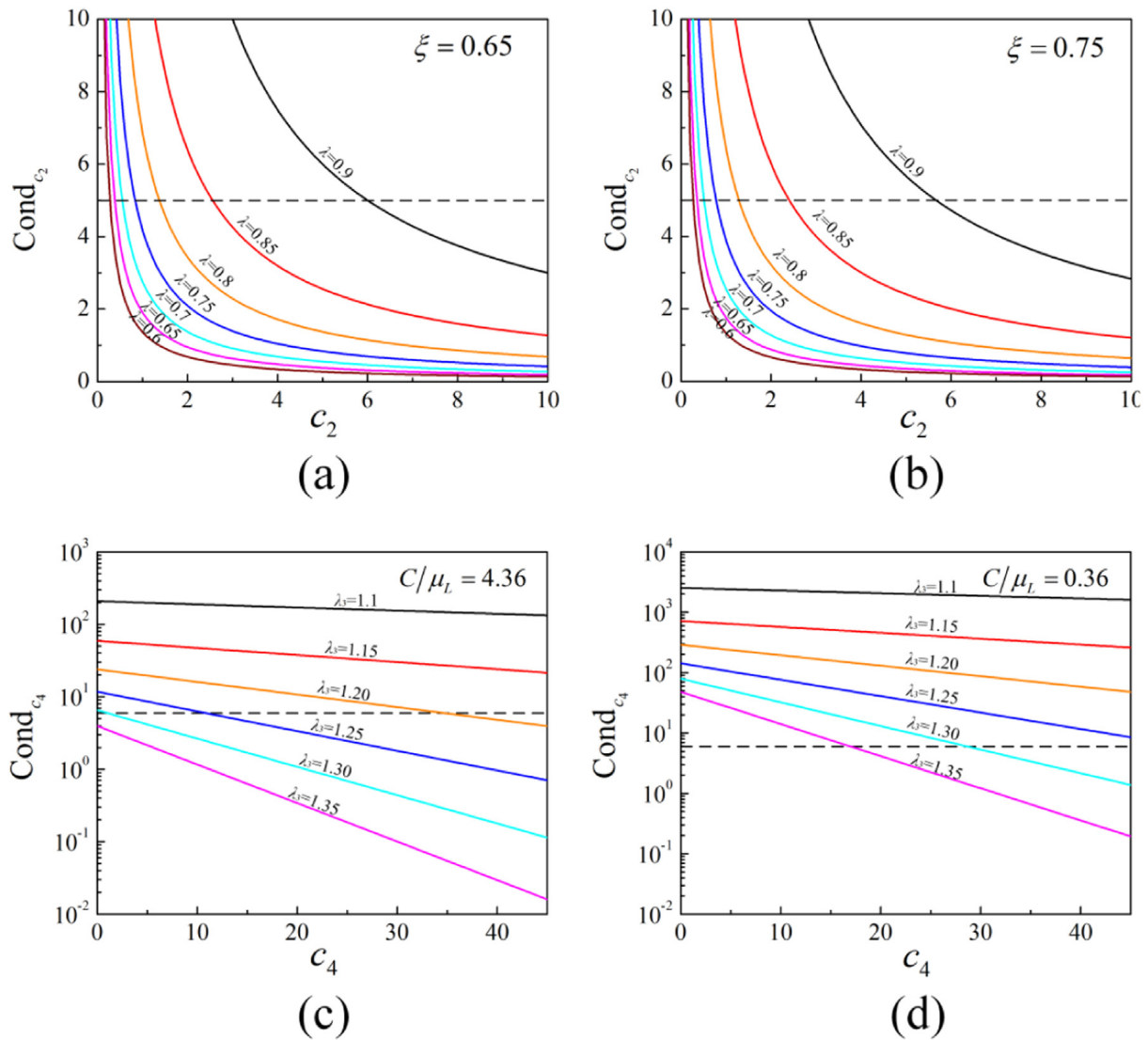


Fig. 13. Plot of the condition number for c_2 and c_4 . (a) $\xi = 0.65$, and (b) $\xi = 0.75$. The parameters adopted are (c) $C/\mu_L = 4.36$ and (d) $C/\mu_L = 0.36$.

enabled us to address the extent to which the identified solutions are sensitive to data errors. The numerical experiments indicate that, besides μ_T and μ_L , the material parameter E_L can also be reliably determined by using the proposed inverse method.

This study focused on the ECE in an incompressible TI solid. Understanding the ECE in general anisotropic solids is by no means trivial because of the complexity of the dynamic Green function and the challenge in building the computational models. This issue is of great importance considering that the SSI technique may be used to characterize soft tissues obeying other anisotropic models. Besides, this paper was concerned with the body wave induced by ARF. The propagation of surface waves on an isotropic or anisotropic elastic half-space has received considerable attention in the literature (Achenbach, 1973; Fu et al., 2013). The investigation of the surface waves induced by the moving ARF is important for characterizing the superficial properties of soft tissues and warrants further research.

Acknowledgments

YPC acknowledges the financial support from the National Natural Science Foundation of China (Grant nos. 11172155 and 11432008).

Appendix A. Supplementary material

Supplementary data associated with this article can be found in the online version at <http://dx.doi.org/10.1016/j.jmps.2016.05.023>.

References

- Achenbach, J.D., 1973. *Wave Propagation in Elastic Solids*. North-Holland Publishing Company, Amsterdam.
- Aki, K., Richards, P.G., 2002. *Quantitative Seismology*. University Science Books, Sausalito, CA.
- Asaro, R.J., Hirth, J.P., Barnett, D.M., Lothe, J., 1973. Further synthesis of sextic and integral theories for dislocations and line forces in anisotropic media. *Phys. Status Solidi B* 60, 261–271.
- Athanasiou, A., Tardivon, A., Tanter, M., Sigal-Zafrani, B., Bercoff, J., Deffieux, T., Gennisson, J.L., Fink, M., Neuenschwander, S., 2010. Breast lesions: quantitative elastography with supersonic shear imaging—preliminary results. *Radiology* 256, 297–303.
- Auld, B.A., 1990. *Acoustic Fields and Waves in Solids*, 2. R.E. Krieger, Florida.
- Bavu, E., Gennisson, J.L., Couade, M., Bercoff, J., Mallet, V., Fink, M., Badel, A., Vallet-Pichard, A., Nalpas, B., Tanter, M., Pol, S., 2011. Noninvasive in vivo liver fibrosis evaluation using supersonic shear imaging: a clinical study on 113 Hepatitis C virus patients. *Ultrasound Med. Biol.* 37, 1361–1373.
- Bercoff, J., Tanter, M., Fink, M., 2004a. Supersonic shear imaging: a new technique for soft tissue elasticity mapping. *IEEE Trans. Ultrason. Ferr.* 51, 396–409.
- Bercoff, J., Tanter, M., Fink, M., 2004b. Sonic boom in soft materials: the elastic Cherenkov effect. *Appl. Phys. Lett.* 84, 2202–2204.
- Biot, M.A., 1940. The influence of initial stress on elastic waves. *J. Appl. Phys.* 11, 522–530.
- Bota, S., Herkner, H., Sporea, I., Salzl, P., Sirlu, R., Neghina, A.M., Peck-Radosavljevic, M., 2013. Meta-analysis: ARFI elastography versus transient elastography for the evaluation of liver fibrosis. *Liver Int.* 33, 1138–1147.
- Brillouin, L., 1925. Sur les tensions de radiation. *Ann. Phys. Sér.* 10 (4), 528–586.
- Carcione, J.M., 2007. *Wave Fields in Real Media: Wave Propagation in Anisotropic, Anelastic, Porous and Electromagnetic Media*. Elsevier, Amsterdam.
- Cassinotto, C., Lapuyade, B., Ait-Ali, A., Vergniol, J., Gaye, D., Foucher, J., Bailacq-Auder, C., Chermak, F., Le Bail, B., de Lédighen, V., 2013. Liver fibrosis: noninvasive assessment with acoustic radiation force impulse elastography—comparison with FibroScan M and XL probes and FibroTest in patients with chronic liver disease. *Radiology* 269, 283–292.
- Chadwick, P., 1993. Wave propagation in incompressible transversely isotropic elastic media. I. Homogeneous plane waves. *Proc. R. Ir. Acad.* 93A, 231–253.
- Chamming's, F., Latorre-Ossa, H., Le Frère-Belda, M.A., Fitoussi, V., Quibel, T., Assayag, F., Marangoni, E., Autret, G., Balvay, D., Pidial, L., Gennisson, J.L., Tanter, M., Cuenod, C.A., Clément, O., Fournier, L.S., 2013. Shear wave elastography of tumour growth in a human breast cancer model with pathological correlation. *Eur. Radiol.* 23, 2079–2086.
- Chen, S., Urban, M.W., Pislaru, C., Kinnick, R., Greenleaf, J.F., 2009b. Liver elasticity and viscosity quantification using shearwave dispersion ultrasound vibrometry (SDUV). *Conf. Proc. IEEE Eng. Med. Biol. Soc.* 2009, 2252–2255.
- Chen, S., Urban, M.W., Pislaru, C., Kinnick, R., Zheng, Y., Yao, A., Greenleaf, J.F., 2009a. Shearwave dispersion ultrasound vibrometry (SDUV) for measuring tissue elasticity and viscosity. *IEEE Trans. Ultrason. Ferroelectr. Freq. Control* 56, 55–62.
- Destrade, M., 2015. Incremental equations for soft fibrous materials. In: Dorfmann, L., Ogden, R.W. (Eds.), *Nonlinear Mechanics of Soft Fibrous Materials*, 559. CISM Lectures Notes, Springer, Wien, pp. 233–267.
- Destrade, M., Ogden, R.W., 2010b. On the third- and fourth-order constants of incompressible isotropic elasticity. *J. Acoust. Soc. Am.* 128, 3334–3343.
- Destrade, M., Martin, P.A., Ting, T.C.T., 2002. The incompressible limit in linear anisotropic elasticity, with applications to surface waves and elastostatics. *J. Mech. Phys. Solids* 50, 1453–1468.
- Destrade, M., Gilchrist, M.D., Ogden, R.W., 2010a. Third- and fourth-order elasticity of biological soft tissues. *J. Acoust. Soc. Am.* 127, 2103–2106.
- Destrade, M., Mac Donald, B., Murphy, J.G., Saccomandi, G., 2013. At least three invariants are necessary to model the mechanical response of incompressible, transversely isotropic materials. *Comput. Mech.* 52, 959–969.
- Dowling, A.P., Williams, J.E., 1983. *Sound and Sources of Sound*. Ellis Horwood, Chichester.
- Eason, G., Fulton, J., Sneddon, I.N., 1956. The generation of waves in an infinite elastic body by variable body forces. *Philos. Trans. R. Soc. A* 248, 575–607.
- Eby, S.F., Cloud, B.A., Brandenburg, J.E., Giambini, H., Song, P.F., Chen, S.G., LeBrasseur, N.K., An, K.N., 2015. Shear wave elastography of passive skeletal muscle stiffness: influences of sex and age throughout adulthood. *Clin. Biomech.* 30, 22–27.
- Fatemi, M., Greenleaf, J.F., 1998. Ultrasound-stimulated vibro-acoustic spectrography. *Science* 280, 82–85.
- Ferraioli, G., Tinelli, C., Dal Bello, B., Zicchetti, M., Filice, G., Filice, C., 2012. Accuracy of real-time shear wave elastography for assessing liver fibrosis in chronic Hepatitis C: a pilot study. *Hepatology* 56, 2125–2133.
- Fu, Y.B., Rogerson, G.A., Wang, W.F., 2013. Surface waves guided by topography in an anisotropic elastic half-space. *Proc. R. Soc. A* 469, 20120371.
- Gennisson, J.L., Grenier, N., Combe, C., Tanter, M., 2012. Supersonic shear wave elastography of in vivo pig kidney: Influence of blood pressure, urinary pressure and tissue anisotropy. *Ultrason. Med. Biol.* 38, 1559–1567.
- Gennisson, J.L., Deffieux, T., Macé, E., Montaldo, G., Fink, M., Tanter, M., 2010. Viscoelasticity and anisotropic mechanical properties of in vivo muscle tissue assessed by supersonic shear imaging. *Ultrason. Med. Biol.* 36, 789–801.
- Gennisson, J.L., Rénier, M., Catheline, S., Barrière, C., Bercoff, J., Tanter, M., Fink, M., 2007. Acoustoelasticity in soft solids: assessment of the nonlinear shear modulus with the acoustic radiation force. *J. Acoust. Soc. Am.* 122, 3211–3219.
- Hadamard, J., 1903. *Leçons sur la Propagation des Ondes et Equations de l'Hydrodynamique*. Hermann.
- Humphrey, J.D., Yin, F.C., 1987. A new constitutive formulation for characterizing the mechanical behavior of soft tissues. *Biophys. J.* 52, 563–570.
- Iovane, G., Nasedkin, A.V., Passarella, F., 2004. Fundamental solutions in antiplane elastodynamic problem for anisotropic medium under moving oscillating source. *Eur. J. Mech. A/Solid* 23, 935–943.
- Iovane, G., Nasedkin, A.V., Passarella, F., 2005. Moving oscillating loads in 2D anisotropic elastic medium: plane waves and fundamental solutions. *Wave Motion* 43, 51–66.
- Jiang, Y., Li, G.Y., Qian, L.X., Liang, S., Destrade, M., Cao, Y.P., 2015b. Measuring the linear and nonlinear elastic properties of brain tissue with shear waves and inverse analysis. *Biomech. Model Mechanobiol.* 14, 1119–1128.
- Jiang, Y., Li, G.Y., Qian, L.X., Hu, X.D., Liu, D., Liang, S., Cao, Y.P., 2015a. Characterization of the nonlinear elastic properties of soft tissues using the supersonic shear imaging (SSI) technique: inverse method, ex vivo and in vivo experiments. *Med. Image Anal.* 20, 97–111.
- Landau, L.D., Lifshitz, E.M., 1986. *Theory of Elasticity*. Butterworth-Heinemann, Oxford.
- Latorre-Ossa, H., Gennisson, J.L., De Brosses, E., Tanter, M., 2012. Quantitative imaging of nonlinear shear modulus by combining static elastography and shear wave elastography. *IEEE Trans. Ultrason. Ferroelectr. Freq. Control* 59, 833–839.
- Lee, W.N., Pernot, M., Couade, M., Messas, E., Bruneval, P., Bel, A., Hagège, A.A., Fink, M., Tanter, M., 2012. Mapping myocardial fiber orientation using echocardiography-based shear wave imaging. *IEEE Med. Imaging* 31, 554–562.
- Li, G.Y., He, Q., Qian, L.X., Liang, S., Liu, Y.L., Yang, X.Y., Luo, J.W., Cao, Y.P., 2016. Elastic Cherenkov effect in transversely isotropic soft materials-II: ex vivo and in vivo experiments. *J. Mech. Phys. Solids* 94, 181–190.
- Luo, C.C., Qian, L.X., Li, G.Y., Jiang, Y., Liang, S., Cao, Y.P., 2015. Determining the in vivo elastic properties of dermis layer of human skin using the supersonic shear imaging technique and inverse analysis. *Med. Phys.* 42, 4106–4115.
- McLaughlin, J., Renzi, D., 2006. Using level set based inversion of arrival times to recover shear wave speed in transient elastography and supersonic imaging. *Inverse Probl.* 22, 707–725.

- Melzer, A., Nunomura, S., Samsonov, D., Ma, Z.W., Goree, J., 2000. Laser-excited Mach cones in a dusty plasma crystal. *Phys. Rev. E* 62, 4162–4176.
- Merodio, J., Ogden, R.W., 2003. Instabilities and loss of ellipticity in fiber-reinforced compressible non-linearly elastic solids under plane deformation. *Int. J. Solids Struct.* 40, 4707–4727.
- Merodio, J., Ogden, R.W., 2005. Mechanical response of fiber-reinforced incompressible non-linearly elastic solids. *Int. J. Nonlinear Mech.* 40, 213–227.
- Murphy, J.G., 2013. Transversely isotropic biological, soft tissue must be modelled using both anisotropic invariants. *Eur. J. Mech. A/Solids* 42, 90–96.
- Nightingale, K., Soo, M.S., Nightingale, R., Trahey, G., 2002. Acoustic radiation force impulse imaging: in vivo demonstration of clinical feasibility. *Ultrasound Med. Biol.* 28, 227–235.
- Nosenko, V., Goree, J., Ma, Z.W., Piel, A., 2002. Observation of shear-wave Mach cones in a 2D dusty-plasma crystal. *Phys. Rev. Lett.* 88.
- Ogden, R.W., Singh, B., 2011. Propagation of waves in an incompressible transversely isotropic elastic solid with initial stress: Biot revisited. *J. Mech. Mater. Struct.* 6, 453–477.
- Ogden, R.W., 2007. Incremental statics and dynamics of pre-stressed elastic materials. In: *Waves in Nonlinear Pre-stressed Materials*, Springer Vienna, pp. 1–26.
- Palmeri, M.L., Sharma, A.C., Bouchard, R.R., Nightingale, R.W., Nightingale, K.R., 2005. A finite-element method model of soft tissue response to impulsive acoustic radiation force. *IEEE Trans. Ultrason. Ferroelectr. Freq. Control* 52, 1699.
- Paparo, F., Corradi, F., Cevasco, L., Revelli, M., Marziano, A., Molini, L., Cenderello, G., Cassola, G., Rollandi, G.A., 2014. Real-time elastography in the assessment of liver fibrosis: a review of qualitative and semi-quantitative methods for elastogram analysis. *Ultrasound Med. Biol.* 40, 1923–1933.
- Papazoglou, S., Rump, J., Braun, J., Sack, I., 2006. Shear wave group velocity inversion in MR elastography of human skeletal muscle. *Magn. Reson. Med* 56, 489–497.
- Rabaud, M., Moisy, F., 2013. Ship Wakes: Kelvin or Mach Angle? *Phys. Rev. Lett.* 110, 214503.
- Rénier, M., Gennisson, J.L., Barrière, C., Royer, D., Fink, M., 2008. Fourth-order shear elastic constant assessment in quasi-incompressible soft solids. *Appl. Phys. Lett.* 93, 101912.
- Rouze, N.C., Wang, M.H., Palmeri, M.L., Nightingale, K.R., 2013. Finite element modeling of impulsive excitation and shear wave propagation in an incompressible, transversely isotropic medium. *J. Biomech.* 46, 2761–2768.
- Samir, A.E., Allegretti, A.S., Zhu, Q.L., Dhyani, M., Anvari, A., Sullivan, D.A., Trottier, C.A., Dougherty, S., Williams, W.W., Babitt, J.L., Wenger, J., Thadhani, R.I., Lin, H.Y., 2015. Shear wave elastography in chronic kidney disease: a pilot experience in native kidneys. *BMC Nephrol.* 16, 119.
- Sarvazyan, A.P., Rudenko, O.V., Swanson, S.D., Fowlkes, J.B., Emelianov, S.Y., 1998. Shear wave elasticity imaging: a new ultrasonic technology of medical diagnostics. *Ultrasound Med. Biol.* 24, 1419–1435.
- Song, P., Zhao, H., Manduca, A., Urban, M.W., Greenleaf, J.F., Chen, S., 2012. Comb-push ultrasound shear elastography (CUSE): a novel method for two-dimensional shear elasticity imaging of soft tissues. *IEEE Trans. Med. Imaging* 31, 1821–1832.
- Song, P., Macdonald, M., Behler, R., Lanning, J., Wang, M., Urban, M., Manduca, A., Zhao, H., Callstrom, M., Alizad, A., Greenleaf, J., Chen, S., 2015. Two-dimensional shear-wave elastography on conventional ultrasound scanners with time-aligned sequential tracking (TAST) and comb-push ultrasound shear elastography (CUSE). *IEEE Trans. Ultrason. Ferroelectr. Freq. Control* 62, 290–302.
- Spencer, A.J.M., 1984. Constitutive theory for strongly anisotropic solids. Spencer, A.J.M. (Ed.), *Continuum Theory of the Mechanics of Fibre-Reinforced Composites*, 282. CISM Lecture Notes, Springer, Wien, pp. 1–72.
- Stroh, A.N., 1962. Steady state problem in anisotropic elasticity. *J. Math. Phys.* 41, 77–103.
- Tanter, M., Bercoff, J., Athanasiou, A., Deffieux, T., Gennisson, J.L., Montaldo, G., Muller, M., Tardivon, A., Fink, M., 2008. Quantitative assessment of breast lesion viscoelasticity: initial clinical results using supersonic shear imaging. *Ultrasound Med. Biol.* 34, 1373–1386.
- Thomsen, L., 1986. Weak elastic anisotropy. *Geophysics* 51, 1954–1966.
- Ting, T.C.T., 1996. *Anisotropic Elasticity. Theory and Applications*. Oxford University Press, Oxford.
- Vavryčuk, V., 2001. Exact elastodynamic Green functions for simple types of anisotropy derived from high-order ray theory. *Stud. Geophys. Geod.* 45, 67–84.
- Wang, C.Y., Achenbach, J.D., 1994. Elastodynamic fundamental solutions for anisotropic solids. *Geophys. J. Int.* 118, 384–392.
- Wu, K.C., 2002. A non-uniformly moving line force in an anisotropic elastic solid. *Proc. R. Soc. A* 45, 1761–1772.